Instrument Science Report WFC3 2014-04

WFC3 Cycle 19 & 20 Dark Calibration: Part I

J. Biretta and M. Bourque
April 10, 2014

ABSTRACT

We summarize work on the WFC3/UVIS dark calibration between Nov. 2011 and Nov. 2013. Three different procedures were used during this time to generate three different flavors of reference file. Type 1 processing used un-flashed dark frames and files were typically delivered several months after observations. Type 2 processing emphasizes rapid processing and delivery of files -- the files are nearly identical to Type 1, but are delivered ~2 weeks after observations. This was used for data taken between Feb. 29 and Nov. 8, 2012. Type 3 processing uses post-flashed raw dark frames, has greatly reduced CTE effects, and are being delivered for observations taken after Nov. 8, 2012. The resulting 196 dark reference files and their properties are tabulated. CTE has a very large effect on the early Type 1 and 2 dark frames. By the end of Cycle 19 image regions farthest from the CCD amplifier lose about ¾ of their hot pixels during read out. Post-flashing in the Type 3 files reduces these losses to about ~40% for Cycle 20 data. We examine the evolution of the dark current. After allowing for CTE effects, the short-term growth rate of "temporary" hot pixels (i.e. correctable by annealing) is constant at ~0.4% per month, while the long-term growth rate of permanent hot pixels is ~0.5% per year. The median (background) dark current at the start of the WFC3 mission is ~2 e-/hr/pixel and increases to ~6 e-/hr/pixel by the end of Cycle 20. We note that two monthly anneals failed to remove hot pixels but caused no long-term ill effects on the detector. Many areas for future improvement are identified, including further automation, lowering the threshold for including hot pixels in reference files, improvements related to CTE effects, and improved dark current monitoring.

Table of Contents

Introduction

CCD detectors exhibit dark current where detector pixels register some non-zero count rate even in the absence of any illumination. Typically there are small numbers of so-called "hot pixels" with a high dark current, a middle ground of so-called "warm pixels," and a weak uniform (or background) dark current component. Radiation damage to the detector caused by high-energy particles in the space environment causes new hot pixels to appear over time. In an effort to correct this, monthly anneal procedures[1] are performed where the CCD detectors are briefly warmed-up from the operating temperature of -82C to ~20C; this has the effect of removing most of the hot pixels (i.e. removing "temporary hot pixels"), but a population of "permanent" hot pixels remains and grows over time.

The dark current in science images is typically corrected by taking dark frames, and subtracting these from the science image. The WFC3 team at STScI takes several dark frames each day and processes these into calibration reference files (images of the dark current) which give the dark current in each pixel (in e-/sec). During pipeline calibration of science images, these reference files are scaled by the exposure time, and subtracted from the science data. A new dark reference file is generated every few days to track the ever-changing population of hot pixels.

Martel, et al., 2009 and Borders, et al., 2009 describe the generation of early dark reference files for WFC3 data based on pre-launch laboratory tests of the instrument. While these reference files are no longer used for current science data, many of the procedures used to generate those files remain the same. Borders and Baggett 2009 describe the first dark reference files made from post-launch data taken during the initial on-orbit testing of WFC3 (SMOV).

Herein we describe the properties of dark frames, procedures used to generate dark reference files, and improvements to the dark calibration made during HST Cycles 19 and 20. A primary goal was to reduce the time delay between observation and delivery of the reference files. In the course of our work we have also noted that CTE (charge transfer efficiency) problems in the CCD detectors were having a large impact on the quality of the dark reference files, and we have taken steps to reduce these effects by post-flashing the raw dark frames.

Subsequent sections herein describe the dark calibration observations and the proposals used to obtain the data, and the detailed procedures for creating dark reference files. We describe three different distinct procedures used for creating dark reference files during Cycles 19 and 20, with each being an improvement over the previous procedure. We list details of the 196

[1] Anneal dates are listed at http://www.stsci.edu/hst/wfc3/ins_performance/monitoring/UVIS/anneal.html

dark reference files produced, and examine their properties as well as those of the input raw dark frames, and the long-term evolution of the dark current. Finally we discuss a wide range of further improvements to the dark calibration that could be made in the future. We discuss calibration for only full-format un-binned data; calibration for binned data is left to other workers.

Part II of this report, which is published separately as WFC3 Technical Instrument Report 2014-01, gives Appendicies containing detailed instructions and scripts for generating the dark reference files.

Calibration Observations and Proposals

The dark calibration is based on 900 second dark frames that are taken daily on-orbit, so as to track the rapidly evolving population of hot pixels in the CCD detector. This exposure time is near that of the longest typical science exposures, and hence should be representative of the dark current in long science exposures which are most susceptible to the dark current. It is also a short enough exposure so that cosmic rays have a relatively minor impact, and can be addressed by combining modest numbers of dark frames. The default nominal CCD gain of 1.5 is used for all dark frames.

The proposals used for dark calibration are listed in Table 1. The observation strategy represents a compromise between thoroughly monitoring the ever-changing hot pixel population in the detectors, maximizing observation efficiency, and minimizing impact on the scheduling of science observations.

In Cycle 19, typically five dark frames are taken at the start of an anneal cycle, shortly after the CCD is returned to its cold operating temperature, by one of the Anneal proposals (12687, 13071, or 13103). These are taken in a single visit, and are interspersed with bias frames. The telescope scheduling is prioritized such that these five dark frames will always be taken prior to the start of science observations in a given anneal cycle. In this way, we are always certain to have a record of the hot pixel population prior to all science images.

Following these initial five frames, dark frames are taken daily by the Daily Monitor program 12689. Typically two to four dark frames are taken per day. The proposal is structured on a four-day cycle that continuously repeats. The first day of the cycle contains a visit with two bias frames, and one dark frame; a second visit contains a pair of back-to-back darks. Day two of the cycle contains two visits, each with two back-to-back dark frames. Day three

contains a single visit with two back-to-back dark frames. And finally day 4 of the cycle contains two more visits, each with two back-to-back dark frames. Hence every four days the Daily Monitor program obtains eleven dark frames, and two bias frames.

And finally the anneal cycle ends with five additional dark frames which are taken by the Anneal proposal. The priority of these darks are set so that they will be the last observations prior to the CCD anneal, and will not be displaced by WFC3 science observations. Hence any WFC3 science observation will be bracketed by dark frames.

At the start of Cycle 20, after the CCD anneal procedure on November 8, 2012, we began to use post-flashed dark frames to reduce CTE effects on the dark calibration. During an initial transition period, we obtained a mixture of post-flashed and un-flashed dark frames. These un-flashed darks would allow continuing the old dark calibration method, in the event that there were un-expected problems with the post-flashed darks. Later in Cycle 20 (in late April 2013), once the viability of post-flashed dark calibration was well established, the un-flashed dark exposures were eliminated.[2] Twelve electron post-flash (FLASH=12) was used at all times; this value was chosen since it has been identified as the "sweet-spot" for reducing CTE effects – it provides a good balance of CTE improvement and minimal noise increase (Anderson, et al., 2012).

Starting after the November 8, 2012 anneal, the CCD Anneal proposal 13071 continues to take five dark frames immediately after the anneal procedure, and five more immediately before the next anneal procedure, but these dark frames are now post-flashed. This proposal also obtains several un-flashed dark frames during the November and December 2012 anneal cycles. The Daily Monitor proposals 13073, 13074, and 13075 continue to use a four-day cycle, but here there are darks both with and without post-flash. Images of the post-flash itself are also included for the purpose of calibrating the post-flash itself. The first day of the cycle contains a visit with two bias frames, a second visit with two post-flashed darks, and a third visit with two un-flashed darks. Day two of the cycle contains two visits, each with two flashed darks, and a third visits with two un-flashed darks. Day three of the cycle obtains two post-flash images (one in each shutter) and a single flashed dark in the first orbit visit; the second visits obtains two flashed darks, and the third visits obtains two un-flashed darks. Day four of the cycle contains two visits, each with two flashed darks, and a final visit with two un-flashed darks. Hence every four days we obtain nine un-flashed darks, and thirteen post-flashed darks, two bias frames, and two post-flash calibration files.

Beginning with visits executed on April 20, 2013, the un-flashed dark frames are dropped

[2] Taking both un-flashed and flashed dark frames together tended to push the limits of the HST schedule, and there were periods where many dark frames were dropped from the HST schedule as a result. Hence we discontinued the un-flashed darks as soon as possible.

from the CCD Daily Monitor proposals, 13073 – 13076. The four day cycle of visits continues, but now the exposures consist of the following. On the first day we obtain two visits – the first has two bias frames and one flashed dark frame, and the second visit contains two flashed darks. On the second day of the cycle we obtain two visits, each with two flashed dark frames. On day three we obtain a visit with two post-flash frames, and one post-flashed dark, and a second visit with two post-flashed darks. And the fourth and final day of the cycle obtains two visits each with two flashed dark frames. Hence every four days we obtain fourteen post-flashed dark frames, two bias frames, and two post-flash calibration files.

While we attempt to schedule several dark frames per day in the Daily Monitor proposals, it is fairly common for some of these exposures to be dropped from the HST schedule to allow scheduling time-critical science observations. Approximately 20% of the planned dark calibration visits were in fact dropped for this reason in proposals 13073 and 13074. After April 2013, when the un-flashed darks are discontinued and we take fewer dark frames, the fraction of dropped dark calibration visits decreases to about 10% (primarily in programs 13075 and 13076).

The orbits in these dropped visits were later re-cycled and used to provide dark calibration during June and July 2013. While most visits in proposals 13073, 13074, and 13075 tended to run in chronological order, each proposal also contains visits in June and July 2013 due to this re-cycling of awarded orbits.[3]

Table 1. Proposals used for dark calibration.

Program ID	Title	PI	Cycle	Internal Orbits Allocated	Observation Date Range
12687	UVIS Anneal	S. Baggett	19	91	14 Oct 2011 – 11 Sep 2012
12689	UVIS CCD Daily Monitor	T. Borders	19	631	2 Nov 2011 – 3 Nov 2012
13071	UVIS Anneal	S. Baggett	20	107	7 Nov 2012 – 11 Oct 2013
13073	UVIS CCD Daily Monitor - A	J. Biretta	20	200	4 Nov 2012 – 19 Jul 2013
13074	UVIS CCD Daily Monitor - B	J. Biretta	20	200	10 Jan – 30 Jun 2013
13075	UVIS CCD Daily Monitor - C	J. Biretta	20	200	17 Mar – 11 Jun 2013
13076	UVIS CCD Daily Monitor - D	J. Biretta	20	205	20 Jul – 1 Nov 2013
13103	UVIS Anneal	S. Baggett	19	13	11-12 Oct 2012

[3] The purpose of this orbit re-cycling was to avoid exceeding the total orbits allocated for dark calibration in Cycle 20. While 805 orbits were allocated, and initially scheduled, we found that many visists were being cancelled at the last minute due to schedule conflicts with science observations. We would then submit additional visits to re-use these allocated orbits – in this way we submitted approximately 1000 orbits of exposures. After all the cancelled visits, the final number of executed orbits was ~805 or about equal to the allocated number.

Procedure for Making Dark Reference Files

During Cycles 19 and 20 three different procedures were used to make dark reference files. Each represents an improvement over the previous procedure, and yields somewhat different reference files. The first type, or *Type 1*, represents the procedure used at the start of Cycle 19. Typically these darks were generated several times per year, so the delay between observation and optimal dark calibration could be many months. *Type 2* or *rapid-delivery darks* represent an effort to minimize the delay between observation and calibration delivery, and hence provide more timely calibration to observers. We began delivering this type of dark reference for data taken after Feb. 29, 2012. Reference files were typically generated and delivered within about 2 weeks of the observations. Finally, *Type 3* or *post-flashed rapid-delivery darks*, are generated from raw darks which are post-flashed on orbit, so as to reduce the effects of CTE losses on calibration and obtain a more accurate correction of hot pixels. Type 3 darks were delivered for all observations taken after Nov 8, 2012 (the approximate start of Cycle 20). These are also delivered within about 2 weeks of the observations. Beginning with data taken after Aug 24, 2013, a variant of the Type 3 processing called *Type 3a* was used. This processing is carried out with automated scripts, but otherwise produces reference files that are identical to the Type 3 reference files. Below we discuss the creation of each type of dark reference file in much greater detail.

Type 1 Processing

Type 1 processing was used from the beginning of Cycle 19 through observations made on Feb 29, 2012.[4] These were generated approximately as follows. Several months after the observations, all 900 sec raw dark frames taken between two CCD anneals were collected – typically there would be 90 to 120 raw dark frames. The files would be collected from WFC3 "Quick-Look" system[5], and then manually selected according to dates and times of the CCD anneals. The files would be calibrated and combined together using CALWF3 (*wfc3_reference.py*[6]). The cosmic ray rejection parameters would be set to SIGMAS = 40,

[4] Ms. Borders left STScI prior to the writing of this report, so the historical details of processing before Feb. 2012 are less certain, but we believe we have accurately described the methods used during that time.

[5] The "Quick-Look" system is s stand-alone pipeline maintained internally by the WFC3 team for archiving, calibrating, and checking WFC3 data.

[6] See Martel, et al., 2008.

39, 38, and CRRADIUS = 0.5 (parameter file *wfc3_uvis_none_crad0.5_sig40_crr.fits*). These parameters are intended to identify and flag the cores of cosmic ray hits, while leaving hot pixels un-flagged.[7] The purpose of using CALWF3 here is simply to flag cosmic rays for each input data set; the combined output file itself is not used. After the cores of cosmic ray hits are flagged, a separate procedure (*noao.imred.crutil.crgrow*) expands the cosmic ray masks, so as to flag pixels surrounding the cosmic ray cores – these pixels will typically be corrupted and have slightly elevated counts due to the nearby cosmic ray.

At this point all the calibrated dark frames are checked by displaying them individually on a high-resolution computer monitor. Frames with missing data, corrupted rows or columns, very large numbers of cosmic rays, etc., are eliminated from further processing (but this is very rare).

Once the dark data files have all been calibrated, they are segregated into 4-day observation periods to create so-called *super-dark* reference files (*superdark_build.py*). Typically there are 7 such time periods between a pair of CCD anneals – the anneals were usually 28 days apart, though sometimes periods up to ~31 days occurred. A 4-day period might typically have 12 to 14 raw dark data files, though the number could range from ~8 to ~16 depending on details of the HST observation schedule. All dark files within the 4-day period were then averaged, while excluding cosmic rays flagged in the data quality mask.

Since these super-darks do not contain large numbers of input files, there is concern that they could add significant noise when used to calibrate deep exposures of astronomical targets. Hence only hot pixels above a threshold are retained, and the rest of the image is set to a constant background level. A threshold of 0.015 e-/sec is used (this corresponds to about 13e- or ~4.5 times the read noise for a single 900 sec CCD image). Pixels above this value are retained as hot pixels. The median value of the rest of the pixels (below the threshold) is computed, and these pixels are then replaced with a constant value which equals the median.

As part of this procedure, we also make plots of the number of hot pixels, and the background dark current, as a function of epoch. These plots serve to point out any processing issues with the new dark reference files, and allow study of long-term trends or health issues in the CCD detectors. The hot pixel plots are made by simply computing the percent of pixels in the calibrated dark frames which are above a threshold of 9 counts[8] (with rejection of pixels

---

[7] This utilizes the fact that the cosmic ray cores (pixels directly hit by cosmic rays) are very bright and always exceed ~250 counts. Surrounding pixels with weaker effects from cosmic rays are dealt with separately by expanding or "growing" the cosmic ray mask.

[8] This equates to a threshold rate of ~56 e-/hr for a nominal gain of 1.56 for these 900 s exposures.

flagged as cosmic rays in the data quality mask, *stats_darks_hotpix.py*).

The background dark current plots use a separate run of CALWF3 where the cosmic ray rejection parameters are set to strongly exclude cosmic rays (and any variable hot pixels) – SIGMAS are set to 6.5, 5.5, 4.5, and CRRADIUS = 2.1 pixels (parameter file *wfc3_uvis_none_crr.fits*). Once the data quality mask has been set using these parameters, the median value of each dark frame is computed (excluding cosmic rays flagged in the data quality mask, and hot pixels brighter than 9 counts).

Besides examining the plots of the numbers of hot pixels and background dark current, each new reference file is displayed on a high resolution monitor, along with its data quality file, prior to delivery .

We do not give detailed instructions for making Type 1 dark reference files, but they would be nearly identical to the instructions listed in Appendix A (see Part II of this report, Biretta 2014, for the Appendicies) for the Type 2 dark reference files. The primary difference is that steps -1 and 0 would be replaced with manual collection of raw darks from a large directory which had been populated by the WFC3 Quick-Look system. The scripts and files would have been more-or-less identical to those listed in Appendix B for Type 2 darks.

Type 2 or "Rapid Delivery" Processing

Type 2, or rapid delivery darks, are generated in a manner very similar to the Type 1 darks, but with several key changes to minimize the delay between observation and delivery of the reference files. This method was used for observations obtained between Feb. 29 and Nov. 8, 2012. Processing for these is done on a weekly basis using all dark frames available for the current anneal cycle. At the start of the anneal cycle, this might mean that processing is done with only a dozen or so dark frames, instead of the 100 or more frames that might be available for Type 1 processing (after the anneal cycle). For example, the initial run of CALWF3 which is used to identify cosmic rays would now be run with far fewer input frames, but a dozen frames is still quite sufficient to accurately identify cosmic rays – it is not necessary to have all ~100 frames to get good results. Hence, it is not necessary to have data from the entire anneal cycle and wait until after the second anneal to generate dark reference files. Good reference files can be made even at the start of the anneal cycle when there are only a few days of data available.

The high-level procedure for making Type 2 dark reference files is as follows: Each week dark reference files are made from all the available dark frames for the current anneal cycle. We

run our procedures on the available data, which then generates some number of dark reference files depending upon where we are in the 28-day anneal cycle. This typically means there are several 4-day segments with complete data, and a final 4-day segment with only partial data available. We would automatically deliver the ones with complete data. The final one with partial data would be delivered only if it contained more than about 7 input dark frames. The following week we would again generate dark reference files using the data then available. Probably there are now more dark frames available for this last 4-day period, and we might re-deliver that last dark reference file, depending on whether many more input dark frames became available. If there were already say 11 dark frames available when it was processed the first week, and only 1 more became available the second week, we might decide not to re-deliver that reference file, since the improvement would be very small.

For example, if we generated dark references files on day 12 of the 28 day anneal cycle, we might have data from only the first 10 days of the cycle. Days 11 and 12 might still be awaiting down-link from HST and initial processing by the HST archive. Hence we would have complete data for days 1-4 and 5-8 of the anneal cycle, and deliver those dark reference files. But the delivery of the dark reference file for days 9-10 would depend on the number of files available. This reference file might possibly be delivered or re-delivered the following week when all data from days 9-12 had become available.

Another change is that the raw dark files were taken directly from the HST archive, and not from the WFC3 Quick-Look system. This tended to simplify the processing and reduced delays[9], though requiring more effort from the operator – the operator must manually query the HST archive for the files each week. All raw dark files from the archive are simply placed into a large directory, and a new script (*copy_d###_Cy##.py*) is used to retrieve specific data files from the directory as needed based on the anneal and observation times.

A third change was that all processing was done on a fast computer with all the data on local disks. This appeared to greatly improve the reliability of the software[10].

We tested the new procedures by processing several anneal cycles using both Type 1 and Type 2 processing, and comparing the resulting dark reference files. For the vast majority of

[9] The WFC3 QuickLook system collects data files immediately after the observations and places them in data directories available to the WFC3 team at STScI. Files that were slightly delayed in normal archive processing would be omitted, and would be recovered several weeks later during re-processing. We found that we could obtain a full set of dark frames more simply and quickly by obtaining them directly from the HST archive.

[10] We experienced sporadic software crashes when using the /grp/hst file server, and these completely went away when a local file system was used instead.

pixels the two methods gave identical values. However, typically there would be in 100 to 200 pixels spread throughout the field of view where the two methods gave different results. Many of these pixels were near the 0.015 e-/sec threshold for retaining them as hot pixels, and would appear as hot pixels only in one file and not the other. Other pixels display complex behavior, and the resulting value depended strongly on exactly which frames were available. Further details of the comparison are given in a later section.

Detailed instructions for making Type 2 dark reference files are given in Appendix A, and the scripts (including the new *copy_d###_Cy##.py* script) are listed in Appendix B (see Part II of this report, Biretta 2014, for the Appendicies).

Type 3 or "Post-Flashed Rapid Delivery" Processing

Type 3 dark reference files use raw dark frames that have been post-flashed on-orbit, so as to minimize CTE effects which occur during readout of the image. Hence these require that post-flash calibration be enabled in CALWF3, so that the post-flash light pattern is removed from the raw dark frames.

We discovered an important feature in CALWF3 which requires that it be run separately on the shutter A and B data. The post-flash is performed by illuminating the backside of the shutters, and hence the resulting light pattern and calibration depends on whether the A or B shutter was in place during the post-flash procedure. There are in fact separate post-flash calibration reference files for the A and B shutters. CALWF3 contains a feature wherein the first post-flash reference file it encounters is used to calibrate all the data. For example, if the first raw dark frame was taken with the A shutter in place, CALWF3 will apply the post-flash reference file for the A shutter to all the data, regardless of the shutter actually used. Hence any raw darks taken in the B shutter receive incorrect calibration and become corrupted. We have devised a work-around which is to begin processing by segregating the shutter A and B data, processing them separately with CALWF3 through the early calibration steps, and then again co-mingling the shutter A and B data for the later processing steps.[11]

The processing for post-flashed dark reference files (Type 3) is otherwise identical to the Type 2 processing, except for turning-on post-flash calibration, and initially segregating the shutter

[11] The CALWF3 "feature" is even more complicated than it seems at first. Its behavior is controlled by the MEMTYPE parameter in the association (ASN) table for the input data. When making dark reference files, MEMTYPE is set to "EXP-CR," and then the first post-flash reference file is used on all the data. However, most science data have MEMTYPE set to "EXP-DTH" and for this setting CALWF3 properly uses the post-flash reference file specified in each input data file header. Hence most science data is correctly processed by CALWF3.

A and B data. Six modified scripts are used to facilitate these changes in the procedure:

```
copy_d###_cy##_pf_a.py
copy_d###_cy##_pf_b.py
ProcessOrbitPFA
ProcessOrbitPFB
wfc3_reference_pf.py
wfc3ref.py
```

Appendix C gives detailed instructions for generating Type 3 dark reference files, including typical messages given by the scripts. Appendix D presents the six modified scripts (see Part II of this report, Biretta 2014, for the Appendicies).

Reference files with USEAFTER dates of Aug 24, 2013 and later were generated with a variant of Type 3 processing we call Type 3a. This utilizes a highly automated script *cal_uvis_make_darks.py* to perform the same processing steps, and will be described in a future report (Bourque, et al., 2014). The reference files generated by Type 3 and Type 3a processing are identical, as has been verified by extensive tests.

Properties of the Dark Frames and Dark Reference Files

Table 2 lists the dark reference files delivered for Cycles 19 and 20. They are ordered by reference file name, which approximately tracks the delivery date.

The second column gives the "USEAFTER" date from the reference file header, which is the first observation date on which a specific file should be used. There is no "use before date," in the headers. Instead a given file should be used until there is a different file with a later USEAFTER date.

The fourth column gives the "Reference File Type" which corresponds to the procedure types 1, 2, 3, and 3a as discussed in the preceding section.

The fifth column in the table gives the number of input dark frames that were averaged to generate the dark reference file. Typically there are 10 to 15 input dark frames. But there are two reference files with as few as 4 input dark frames. These represent time periods where high-priority WFC3 science observations displaced the dark frames on the HST schedule.

Column six gives the staff member responsible for processing the dark frames and generating

the reference file: Tiffany Borders, John Biretta, or Matthew Bourque.

In a few cases there are multiple deliveries with the same USEAFTER date. In these cases the file delivered later should be used. These represent situations where enough additional raw dark frames became available later in the anneal cycle, that we judged the reference file could be significantly improved by re-generating it with the additional input dark frames. For example, the USEAFTER date 4-Jan-2012 has reference files w1p1615pi_drk.fits and w2d1918pi_drk.fits, with 5 and 18 input dark frames, and delivered on 25-Jan-2012 and 13-Feb-2012, respectively. Both cover observations from the same time period, but the later one with 18 input dark frames should be used at this point in time.

Some of the reference files listed at the end of the table extend past the nominal end of Cycle 20, but are included for completeness.

Table 2. Dark reference files delivered for Cycles 19 and 20.

Reference File Name	USEAFTER	Delivery Date	Reference File Type	# Input Darks Frame Averaged	Processed By
w1h22005i_drk.fits	5-Nov-2011	17-Jan-2012	1	14	Borders
w1h22006i_drk.fits	9-Nov-2011	17-Jan-2012	1	12	Borders
w1i2014gi_drk.fits	11-Nov-2011	18-Jan-2012	1	21	Borders
w1i2014hi_drk.fits	16-Nov-2011	18-Jan-2012	1	14	Borders
w1i2014ii_drk.fits	20-Nov-2011	18-Jan-2012	1	14	Borders
w1i2014ji_drk.fits	24-Nov-2011	18-Jan-2012	1	14	Borders
w1i2014ki_drk.fits	28-Nov-2011	18-Jan-2012	1	13	Borders
w1i2014li_drk.fits	2-Dec-2011	18-Jan-2012	1	14	Borders
w1p1615ii_drk.fits	5-Dec-2011	25-Jan-2012	1	18	Borders
w1p1615ji_drk.fits	10-Dec-2011	25-Jan-2012	1	11	Borders
w1p1615ki_drk.fits	14-Dec-2011	25-Jan-2012	1	13	Borders
w1p1615li_drk.fits	18-Dec-2011	25-Jan-2012	1	15	Borders
w1p1615mi_drk.fits	23-Dec-2011	25-Jan-2012	1	11	Borders
w1p1615ni_drk.fits	26-Dec-2011	25-Jan-2012	1	15	Borders
w1p1615oi_drk.fits	31-Dec-2011	25-Jan-2012	1	13	Borders
w1p1615pi_drk.fits	4-Jan-2012	25-Jan-2012	1	5	Borders
w2d1918pi_drk.fits	4-Jan-2012	13-Feb-2012	1	18	Borders
w2d1918qi_drk.fits	9-Jan-2012	13-Feb-2012	1	13	Borders
w2d1918ri_drk.fits	13-Jan-2012	13-Feb-2012	1	14	Borders
w2d1918si_drk.fits	17-Jan-2012	13-Feb-2012	1	15	Borders

w2d1918ti_drk.fits	22-Jan-2012	13-Feb-2012	1	11	Borders
w2d19190i_drk.fits	25-Jan-2012	13-Feb-2012	1	15	Borders
w2d19191i_drk.fits	30-Jan-2012	13-Feb-2012	1	7	Borders
w2d19192i_drk.fits	2-Feb-2012	13-Feb-2012	1	7	Borders
w3e1718gi_drk.fits	4-Feb-2012	14-Mar-2012	1	14	Biretta
w3e1718hi_drk.fits	9-Feb-2012	14-Mar-2012	1	13	Biretta
w3e1718ii_drk.fits	13-Feb-2012	14-Mar-2012	1	13	Biretta
w3e1718ji_drk.fits	17-Feb-2012	14-Mar-2012	1	13	Biretta
w3e1718ki_drk.fits	21-Feb-2012	14-Mar-2012	1	13	Biretta
w3e1718li_drk.fits	25-Feb-2012	14-Mar-2012	1	13	Biretta
w3e1718mi_drk.fits	29-Feb-2012	14-Mar-2012	1	5	Biretta
w3m14445i_drk.fits	29-Feb-2012	22-Mar-2012	2	18	Biretta
w3m14446i_drk.fits	5-Mar-2012	22-Mar-2012	2	13	Biretta
w3m14447i_drk.fits	9-Mar-2012	22-Mar-2012	2	16	Biretta
w3m14448i_drk.fits	14-Mar-2012	22-Mar-2012	2	13	Biretta
w421435hi_drk.fits	18-Mar-2012	2-Apr-2012	2	12	Biretta
w421435ii_drk.fits	21-Mar-2012	2-Apr-2012	2	11	Biretta
w421435ji_drk.fits	25-Mar-2012	2-Apr-2012	2	12	Biretta
w4514023i_drk.fits	28-Mar-2012	5-Apr-2012	2	14	Biretta
w4a15134i_drk.fits	2-Apr-2012	10-Apr-2012	2	13	Biretta
w4j1903ri_drk.fits	6-Apr-2012	19-Apr-2012	2	13	Biretta
w4j1903si_drk.fits	10-Apr-2012	19-Apr-2012	2	8	Biretta
w4o2120ni_drk.fits	14-Apr-2012	24-Apr-2012	2	12	Biretta
w4o2120oi_drk.fits	18-Apr-2012	24-Apr-2012	2	11	Biretta
w5416538i_drk.fits	22-Apr-2012	4-May-2012	2	16	Biretta
w5416539i_drk.fits	25-Apr-2012	4-May-2012	2	20	Biretta
w591925ei_drk.fits	1-May-2012	9-May-2012	2	13	Biretta
w5i1552mi_drk.fits	5-May-2012	18-May-2012	2	13	Biretta
w5n1341si_drk.fits	9-May-2012	23-May-2012	2	13	Biretta
w5n1341ti_drk.fits	13-May-2012	23-May-2012	2	11	Biretta
w5n13420i_drk.fits	17-May-2012	23-May-2012	2	12	Biretta
w5p1345mi_drk.fits	21-May-2012	25-May-2012	2	15	Biretta
w5u17124i_drk.fits	23-May-2012	30-May-2012	2	13	Biretta
w6715010i_drk.fits	28-May-2012	7-Jun-2012	2	13	Biretta
w6c1410ii_drk.fits	1-Jun-2012	12-Jun-2012	2	10	Biretta
w6k0007fi_drk.fits	7-Jun-2012	20-Jun-2012	2	9	Biretta
w6k0007gi_drk.fits	9-Jun-2012	20-Jun-2012	2	13	Biretta
w6k0007hi_drk.fits	14-Jun-2012	20-Jun-2012	2	12	Biretta
w6r1411ki_drk.fits	18-Jun-2012	27-Jun-2012	2	11	Biretta
w751541bi_drk.fits	20-Jun-2012	5-Jul-2012	2	18	Biretta
w7h17547i_drk.fits	25-Jun-2012	17-Jul-2012	2	13	Biretta

w7h17548i_drk.fits	29-Jun-2012	17-Jul-2012	2	13	Biretta
w7h17549i_drk.fits	3-Jul-2012	17-Jul-2012	2	12	Biretta
w811331di_drk.fits	7-Jul-2012	1-Aug-2012	2	13	Biretta
w811331ei_drk.fits	11-Jul-2012	1-Aug-2012	2	13	Biretta
w811331fi_drk.fits	15-Jul-2012	1-Aug-2012	2	12	Biretta
w811331gi_drk.fits	17-Jul-2012	1-Aug-2012	2	17	Biretta
w811331hi_drk.fits	22-Jul-2012	1-Aug-2012	2	14	Biretta
w8a1551ei_drk.fits	26-Jul-2012	10-Aug-2012	2	14	Biretta
w8a1551fi_drk.fits	31-Jul-2012	10-Aug-2012	2	10	Biretta
w8a1551gi_drk.fits	4-Aug-2012	10-Aug-2012	2	13	Biretta
w8u1945di_drk.fits	8-Aug-2012	30-Aug-2012	2	13	Biretta
w8u1945ei_drk.fits	12-Aug-2012	30-Aug-2012	2	11	Biretta
w8v1356pi_drk.fits	15-Aug-2012	31-Aug-2012	2	20	Biretta
w8v1356qi_drk.fits	21-Aug-2012	31-Aug-2012	2	11	Biretta
w8v1356ri_drk.fits	24-Aug-2012	31-Aug-2012	2	12	Biretta
w971325mi_drk.fits	28-Aug-2012	7-Sep-2012	2	12	Biretta
w9k1521si_drk.fits	1-Sep-2012	20-Sep-2012	2	12	Biretta
w9k1521ti_drk.fits	6-Sep-2012	20-Sep-2012	2	13	Biretta
w9k15220i_drk.fits	10-Sep-2012	20-Sep-2012	2	5	Biretta
w9k15221i_drk.fits	11-Sep-2012	20-Sep-2012	2	12	Biretta
w9p1247ni_drk.fits	16-Sep-2012	25-Sep-2012	2	13	Biretta
wb81559li_drk.fits	20-Sep-2012	8-Nov-2012	2	13	Biretta
wb81559mi_drk.fits	24-Sep-2012	8-Nov-2012	2	13	Biretta
wb81559ni_drk.fits	28-Sep-2012	8-Nov-2012	2	12	Biretta
wb81559oi_drk.fits	2-Oct-2012	8-Nov-2012	2	13	Biretta
wb81559pi_drk.fits	6-Oct-2012	8-Nov-2012	2	13	Biretta
wb81559qi_drk.fits	10-Oct-2012	8-Nov-2012	2	10	Biretta
wb81559ri_drk.fits	11-Oct-2012	8-Nov-2012	2	22	Biretta
wb81559si_drk.fits	17-Oct-2012	8-Nov-2012	2	11	Biretta
wb81559ti_drk.fits	20-Oct-2012	8-Nov-2012	2	15	Biretta
wb816000i_drk.fits	25-Oct-2012	8-Nov-2012	2	13	Biretta
wb816001i_drk.fits	29-Oct-2012	8-Nov-2012	2	10	Biretta
x211641hi_drk.fits	8-Nov-2012	1-Feb-2013	3	17	Biretta
x211641ii_drk.fits	12-Nov-2012	1-Feb-2013	3	9	Biretta
x211641ji_drk.fits	17-Nov-2012	1-Feb-2013	3	11	Biretta
x211641ki_drk.fits	21-Nov-2012	1-Feb-2013	3	13	Biretta
x211641li_drk.fits	25-Nov-2012	1-Feb-2013	3	13	Biretta
x211641mi_drk.fits	29-Nov-2012	1-Feb-2013	3	13	Biretta
x211641ni_drk.fits	3-Dec-2012	1-Feb-2013	3	16	Biretta
x2415415i_drk.fits	6-Dec-2012	4-Feb-2013	3	20	Biretta
x2415416i_drk.fits	11-Dec-2012	4-Feb-2013	3	11	Biretta

x2415417i_drk.fits	15-Dec-2012	4-Feb-2013	3	17	Biretta
x2415418i_drk.fits	20-Dec-2012	4-Feb-2013	3	9	Biretta
x2415419i_drk.fits	25-Dec-2012	4-Feb-2013	3	7	Biretta
x241541ai_drk.fits	27-Dec-2012	4-Feb-2013	3	10	Biretta
x241541bi_drk.fits	1-Jan-2013	4-Feb-2013	3	5	Biretta
x281939ti_drk.fits	2-Nov-2012	8-Feb-2013	2	8	Bourque
x2819400i_drk.fits	6-Nov-2012	8-Feb-2013	2	6	Bourque
x2m18485i_drk.fits	1-Jan-2013	22-Feb-2013	3	18	Biretta
x2m18486i_drk.fits	6-Jan-2013	22-Feb-2013	3	11	Biretta
x2m18487i_drk.fits	10-Jan-2013	22-Feb-2013	3	16	Biretta
x2m18488i_drk.fits	15-Jan-2013	22-Feb-2013	3	13	Biretta
x2m18489i_drk.fits	19-Jan-2013	22-Feb-2013	3	10	Biretta
x2m1848ai_drk.fits	22-Jan-2013	22-Feb-2013	3	16	Biretta
x2m1848bi_drk.fits	28-Jan-2013	22-Feb-2013	3	9	Biretta
x2m1848ci_drk.fits	30-Jan-2013	22-Feb-2013	3	5	Biretta
x3q19515i_drk.fits	31-Jan-2013	26-Mar-2013	3	18	Biretta
x3q19516i_drk.fits	5-Feb-2013	26-Mar-2013	3	9	Biretta
x3q19517i_drk.fits	9-Feb-2013	26-Mar-2013	3	9	Biretta
x3q19518i_drk.fits	13-Feb-2013	26-Mar-2013	3	7	Biretta
x3q19519i_drk.fits	20-Feb-2013	26-Mar-2013	3	4	Biretta
x3q1951ai_drk.fits	21-Feb-2013	26-Mar-2013	3	11	Biretta
x3q1951bi_drk.fits	25-Feb-2013	26-Mar-2013	3	10	Biretta
x441617fi_drk.fits	28-Feb-2013	4-Apr-2013	3	18	Bourque
x441617gi_drk.fits	5-Mar-2013	4-Apr-2013	3	13	Bourque
x441617hi_drk.fits	9-Mar-2013	4-Apr-2013	3	14	Bourque
x441617ii_drk.fits	13-Mar-2013	4-Apr-2013	3	12	Bourque
x441617ji_drk.fits	17-Mar-2013	4-Apr-2013	3	11	Bourque
x441617ki_drk.fits	21-Mar-2013	4-Apr-2013	3	13	Bourque
x441617li_drk.fits	25-Mar-2013	4-Apr-2013	3	7	Bourque
x4b1402ni_drk.fits	26-Mar-2013	11-Apr-2013	3	19	Bourque
x4g20208i_drk.fits	31-Mar-2013	16-Apr-2013	3	15	Bourque
x4g20209i_drk.fits	5-Apr-2013	16-Apr-2013	3	12	Bourque
x4g2020ai_drk.fits	9-Apr-2013	16-Apr-2013	3	8	Bourque
x4q1440ni_drk.fits	13-Apr-2013	26-Apr-2013	3	13	Bourque
x4q1440oi_drk.fits	17-Apr-2013	26-Apr-2013	3	8	Bourque
x561646ti_drk.fits	20-Apr-2013	6-May-2013	3	15	Bourque
x5616470i_drk.fits	25-Apr-2013	6-May-2013	3	7	Bourque
x5616471i_drk.fits	26-Apr-2013	6-May-2013	3	19	Bourque
x5616472i_drk.fits	1-May-2013	6-May-2013	3	14	Bourque
x5f17144i_drk.fits	5-May-2013	15-May-2013	3	12	Bourque
x5f17145i_drk.fits	9-May-2013	15-May-2013	3	12	Bourque

x6a2036di_drk.fits	13-May-2013	10-Jun-2013	3	12	Bourque
x6a2036ei_drk.fits	17-May-2013	10-Jun-2013	3	13	Bourque
x6a2036fi_drk.fits	21-May-2013	10-Jun-2013	3	9	Bourque
x6a2036gi_drk.fits	22-May-2013	10-Jun-2013	3	21	Bourque
x6a2036hi_drk.fits	28-May-2013	10-Jun-2013	3	10	Bourque
x6a2036ii_drk.fits	1-Jun-2013	10-Jun-2013	3	10	Bourque
x6a2036ji_drk.fits	4-Jun-2013	10-Jun-2013	3	13	Bourque
x6i1712ri_drk.fits	8-Jun-2013	18-Jun-2013	3	14	Bourque
x6i1712si_drk.fits	12-Jun-2013	18-Jun-2013	3	8	Bourque
x721419fi_drk.fits	17-Jun-2013	2-Jul-2013	3	19	Bourque
x721419gi_drk.fits	20-Jun-2013	2-Jul-2013	3	20	Bourque
x721419hi_drk.fits	25-Jun-2013	2-Jul-2013	3	15	Bourque
x7h1457mi_drk.fits	30-Jun-2013	17-Jul-2013	3	4	Bourque
x7h1457ni_drk.fits	4-Jul-2013	17-Jul-2013	3	7	Bourque
x7h1457oi_drk.fits	8-Jul-2013	17-Jul-2013	3	7	Bourque
x7h1457pi_drk.fits	11-Jul-2013	17-Jul-2013	3	17	Bourque
x7v2004ri_drk.fits	16-Jul-2013	31-Jul-2013	3	12	Bourque
x7v2004si_drk.fits	18-Jul-2013	31-Jul-2013	3	17	Bourque
x7v2004ti_drk.fits	24-Jul-2013	31-Jul-2013	3	7	Bourque
x8k1551hi_drk.fits	27-Jul-2013	20-Aug-2013	3	16	Bourque
x8k1551ii_drk.fits	31-Jul-2013	20-Aug-2013	3	10	Bourque
x8k1551ji_drk.fits	4-Aug-2013	20-Aug-2013	3	8	Bourque
x8k1551ki_drk.fits	7-Aug-2013	20-Aug-2013	3	12	Bourque
x8k1551li_drk.fits	12-Aug-2013	20-Aug-2013	3	9	Bourque
x9618368i_drk.fits	15-Aug-2013	6-Sep-2013	3	17	Bourque
x9618369i_drk.fits	20-Aug-2013	6-Sep-2013	3	10	Bourque
x961836ai_drk.fits	24-Aug-2013	6-Sep-2013	3a	10	Bourque
x961836bi_drk.fits	28-Aug-2013	6-Sep-2013	3a	10	Bourque
x9j1644li_drk.fits	1-Sep-2013	19-Sep-2013	3a	10	Bourque
x9j1644mi_drk.fits	5-Sep-2013	19-Sep-2013	3a	14	Bourque
x9j1644ni_drk.fits	9-Sep-2013	19-Sep-2013	3a	15	Bourque
x9j1644oi_drk.fits	12-Sep-2013	19-Sep-2013	3a	13	Bourque
xa913502i_drk.fits	18-Sep-2013	9-Oct-2013	3a	11	Bourque
xa913503i_drk.fits	21-Sep-2013	9-Oct-2013	3a	14	Bourque
xa913504i_drk.fits	25-Sep-2013	9-Oct-2013	3a	12	Bourque
xas1815ei_drk.fits	29-Sep-2013	28-Oct-2013	3a	12	Bourque
xas1815fi_drk.fits	3-Oct-2013	28-Oct-2013	3a	14	Bourque
xas1815gi_drk.fits	7-Oct-2013	28-Oct-2013	3a	18	Bourque
xas1815hi_drk.fits	10-Oct-2013	28-Oct-2013	3a	22	Bourque
xas1815ii_drk.fits	16-Oct-2013	28-Oct-2013	3a	9	Bourque
xas1815ji_drk.fits	19-Oct-2013	28-Oct-2013	3a	17	Bourque

xb61439ti_drk.fits	23-Oct-2013	6-Nov-2013	3a	14	Bourque
xb614400i_drk.fits	28-Oct-2013	6-Nov-2013	3a	11	Bourque
xbi1903pi_drk.fits	1-Nov-2013	18-Nov-2013	3a	11	Bourque
xbi1903qi_drk.fits	5-Nov-2013	18-Nov-2013	3a	10	Bourque
xbi1903ri_drk.fits	9-Nov-2013	18-Nov-2013	3a	9	Bourque
xc21959fi_drk.fits	10-Nov-2013	2-Dec-2013	3a	11	Bourque
xc21959gi_drk.fits	17-Nov-2013	2-Dec-2013	3a	7	Bourque
xc21959hi_drk.fits	19-Nov-2013	2-Dec-2013	3a	11	Bourque
xch16393i_drk.fits	23-Nov-2013	17-Dec-2013	3a	12	Bourque
xch16394i_drk.fits	27-Nov-2013	17-Dec-2013	3a	11	Bourque
xch16395i_drk.fits	30-Nov-2013	17-Dec-2013	3a	17	Bourque
xch16396i_drk.fits	4-Dec-2013	17-Dec-2013	3a	20	Bourque

Type 1 and Type 2 Dark Frames and Reference Files

The properties of the Type 1 and Type 2 reference files are generally similar and will be discussed together. Both begin with raw 900 s dark frames which have no post-flash. The amplifier C region of such a calibrated dark frame is displayed in Figure 1. The features visible in this image are primarily cosmic rays. Enlargements of the regions nearest and farthest from the readout amplifier are shown in Figure 2 and Figure 3. In these enlargements the multi-pixel features are cosmic rays, while the single-pixel features are hot pixels. As expected, the region far from the readout amplifier shows significant vertical trailing due to the effects of CTE losses – both the cosmic rays and brighter hot pixels are trailed. It is also apparent that there are many fewer faint hot pixels far from the amplifier, as compared to the region near the amplifier, and again this is caused by CTE losses – many of the faint hot pixels are being lost during readout.

Properties of the dark frames can be more easily seen if many of them are stacked to reject cosmic rays and improve the signal-to-noise ratio. Figure 4 and Figure 5 show a summed stack of 76 dark frames taken between the Oct. 11 and Nov. 8, 2012 anneals. The region nearest the read-out amplifier is shown in Figure 4. All cosmic rays have been removed and numerous hot pixels remain. Figure 5 shows the region farthest from the amplifier. Here bright hot pixels are strongly trailed due to CTE losses. Unlike Figure 4 the image is relatively devoid of faint hot pixels (warm pixels). There are also many faint vertical trails without an obvious associated hot pixel – these may be trails from cosmic rays where the cosmic ray itself was rejected, but its associated CTE trail still appears in the stack.

One apparent difference between Figure 4 and Figure 5 is that the background dark current is

much higher far from the amplifier. This is likely due to the combined effects of many CTE trails – both from the visible hot pixels, and from cosmic rays which have been rejected during stacking of the dark frames. This situation can be made clearer by plotting the median background level vs. CCD row number, and this is done in Figure 6. The blue values are for the stack of 76 dark frames previously mentioned without post-flash. The median background has been computed for the image taken 100 rows at a time. We see that the background increases from ~0.0007 e-/sec near the read-out amplifier to ~0.0022 e-/sec far from the amplifier.

Figure 7 shows a histogram of hot pixel values for the image shown in Figure 4 and Figure 5. The histogram is for the C amplifier quadrant. For clarity we have only plotted the histogram up to 0.25 e-/sec – there are 1306 pixels brighter than this value (0.03% of the pixels), with the brightest hot pixel having a count rate of 24 e-/sec. The vertical dotted line indicates the limit 0.015 e-/sec above which hot pixels are retained in making the reference files – this comprises only about 0.77% of the pixels. The pixels below this limit – the vast majority of pixels -- are set to a uniform constant value in the dark reference files. This uniform constant value is computed separately for each dark reference file as the median value of the pixels below 0.015 e-/sec.

Enlarged regions of a typical dark reference file are shown in Figure 8 and Figure 9, for regions near and far from the amplifier, respectively. This is reference file wb81559ri_drk.fits, which is contemporary with the images shown in Figure 1 through Figure 5, and can be compared with those. This reference file was generated using Type 2 processing, and contains 22 input dark frames. Both images show numerous hot pixels, while pixels below 0.015 e-/sec have been set to the median background level of 0.0017 e-/sec. The region near the readout amplifier shows many more hot pixels than the region far from the amplifier, due to CTE losses far from the amplifier.

Setting pixels below 0.015 e-/sec to a constant value serves several purposes. One is to minimize noise which is imposed on calibrated science data. But another is apparent from Figure 4 and Figure 5. While the background near the amplifier contains useful information about weak hot pixels, in regions far from the amplifier the background is dominated by artifacts from trailed bright hot pixels and possibly trailed cosmic rays. Imposing a flat background avoids corrupting science data with these artifacts.

The decrease in the number of hot pixels far from the readout amplifier can be quantized by counting the number of hot pixels per CCD row, and plotting them vs. row number. This is done in Figure 10 for this same reference file. We see that the number of hot pixels per row decreases systematically from ~33 near the amplifier, to ~8 in regions farthest from the amplifier. (This corresponds to ~1.6% hot pixels near the amplifier, and ~0.4% far from the

amplifier.) Apparently about three-fourths of the hot pixels are being lost at high row numbers due to CTE losses. These losses of hot pixels provide much of the motivation for transitioning to Type 3 dark reference files where post-flashed dark frames are used.

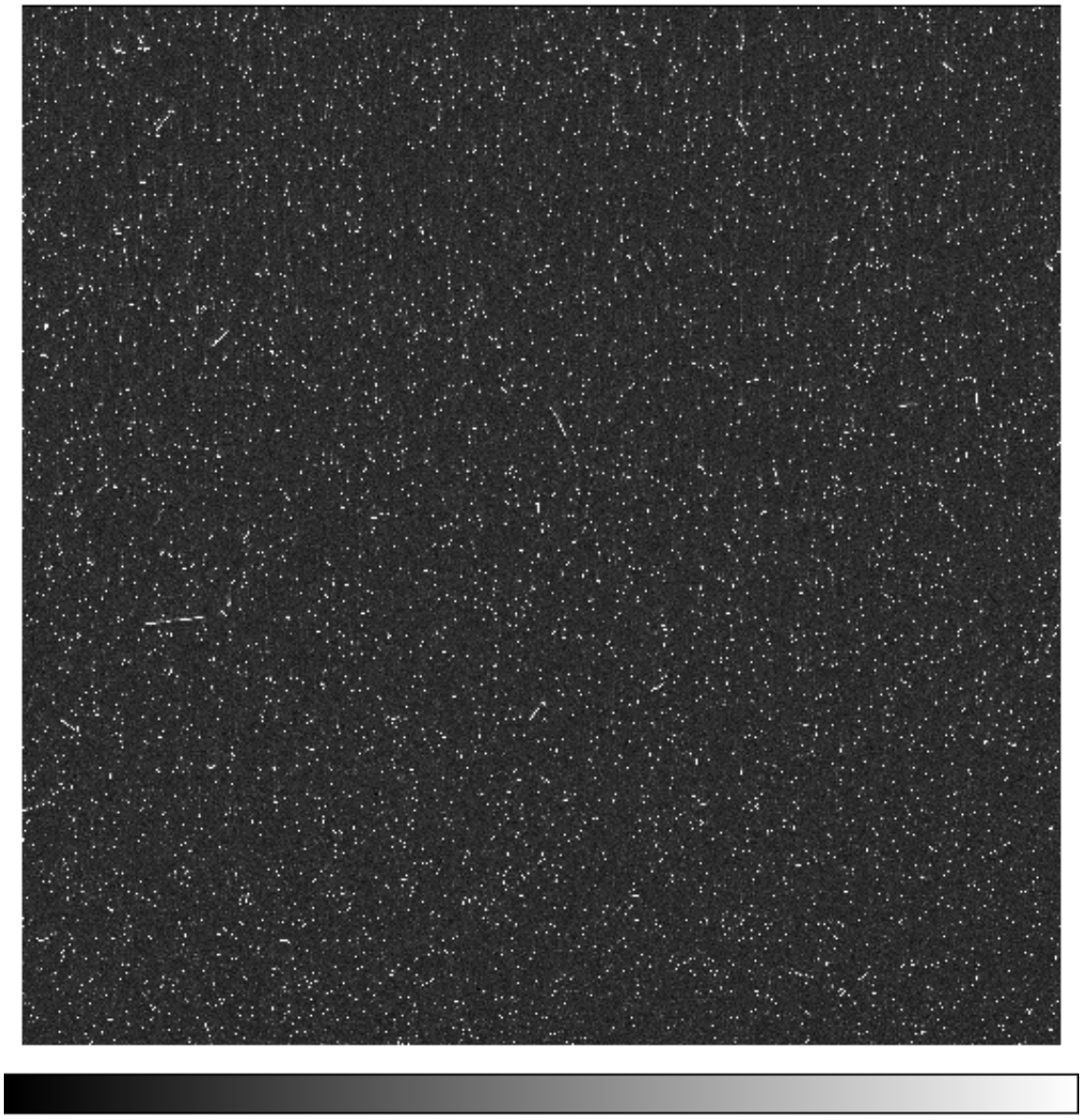

Figure 1. The C quadrant region of a typical calibrated 900s dark frame taken without post-flash on Oct. 12, 2012 (file ibu9gtylq). Virtually all features visible in this display are cosmic rays. The image is 2048 pixels on a side, and the brightness scale runs from -10 to 50 counts.

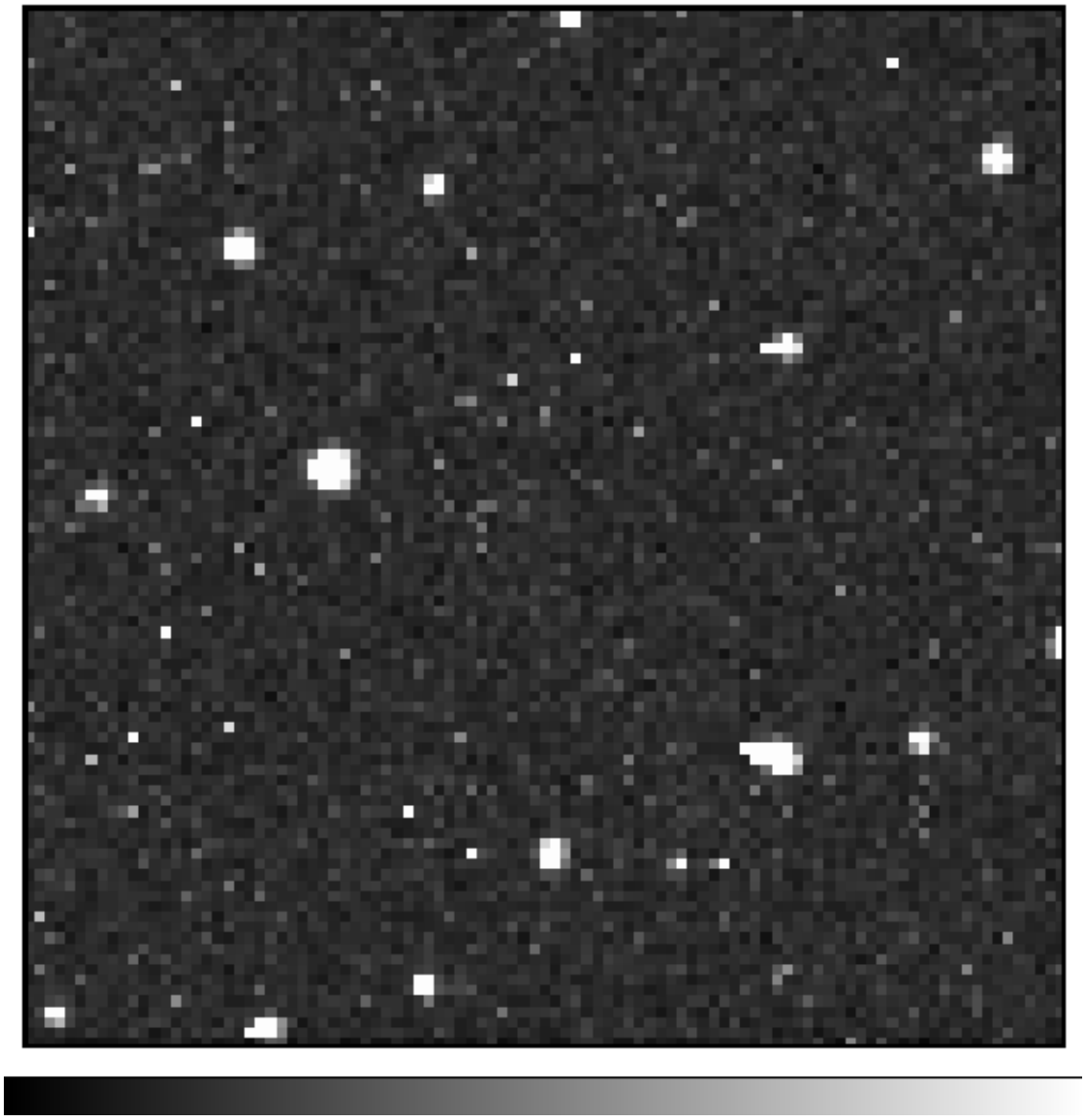

Figure 2. Region of Figure 1 nearest the readout amplifier. This is the C quadrant region of a typical calibrated 900s dark frame taken without post-flash on Oct. 12, 2012 (file ibu9gtylq). Multi-pixel features are cosmic rays, while single pixel features are hot pixels. The image is 100 pixels on a side, and the brightness scale runs from -10 to 50 counts.

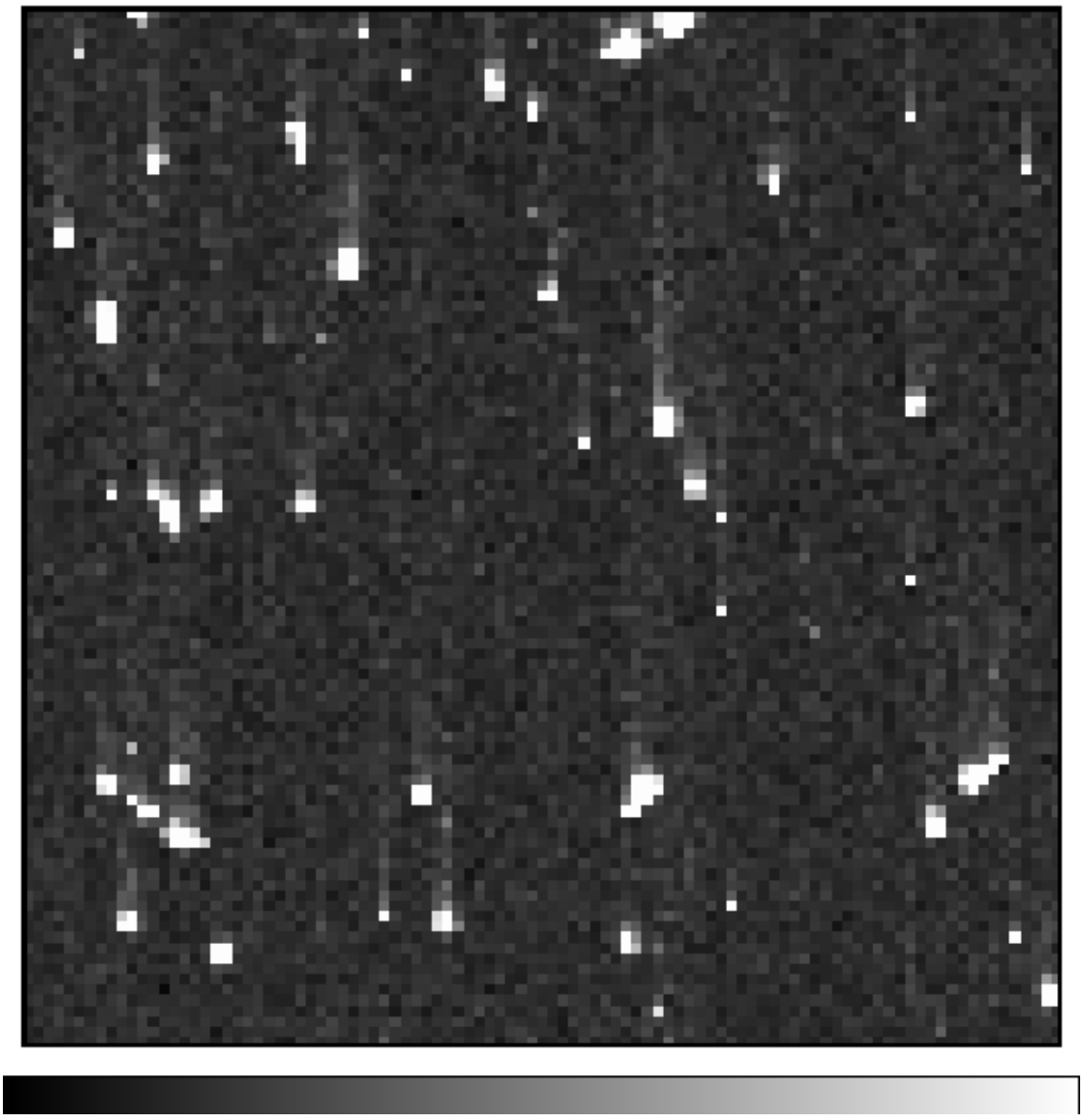

Figure 3. Same image as Figure 1 and Figure 2, but showing the region farthest from the readout amplifier. Multi-pixel features are cosmic rays, while single pixel features are hot pixels. Features are trailed vertically due to CTE issues. There are relatively few faint hot pixels compared to Figure 2. The image is 100 pixels on a side, and the brightness scale runs from -10 to 50 counts.

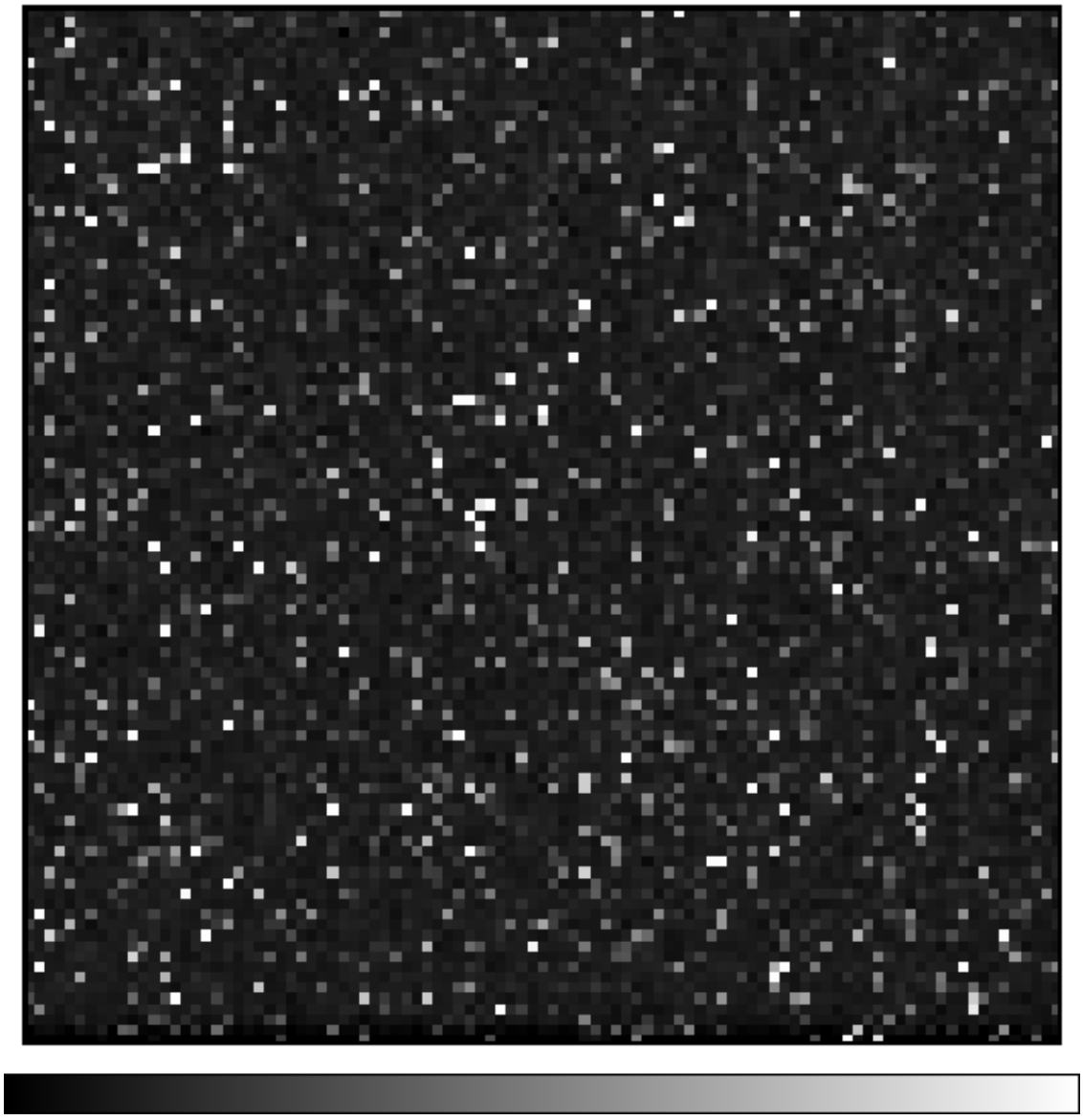

Figure 4. Region near the read-out amplifier of the C quadrant for a summed stack of 76 dark frames taken between the Oct. 11 and Nov. 8, 2012 anneals. Virtually all the visible features are hot and warm pixels. The image is 100 pixels on a side, and the brightness scale runs from -100 to 1000 counts.

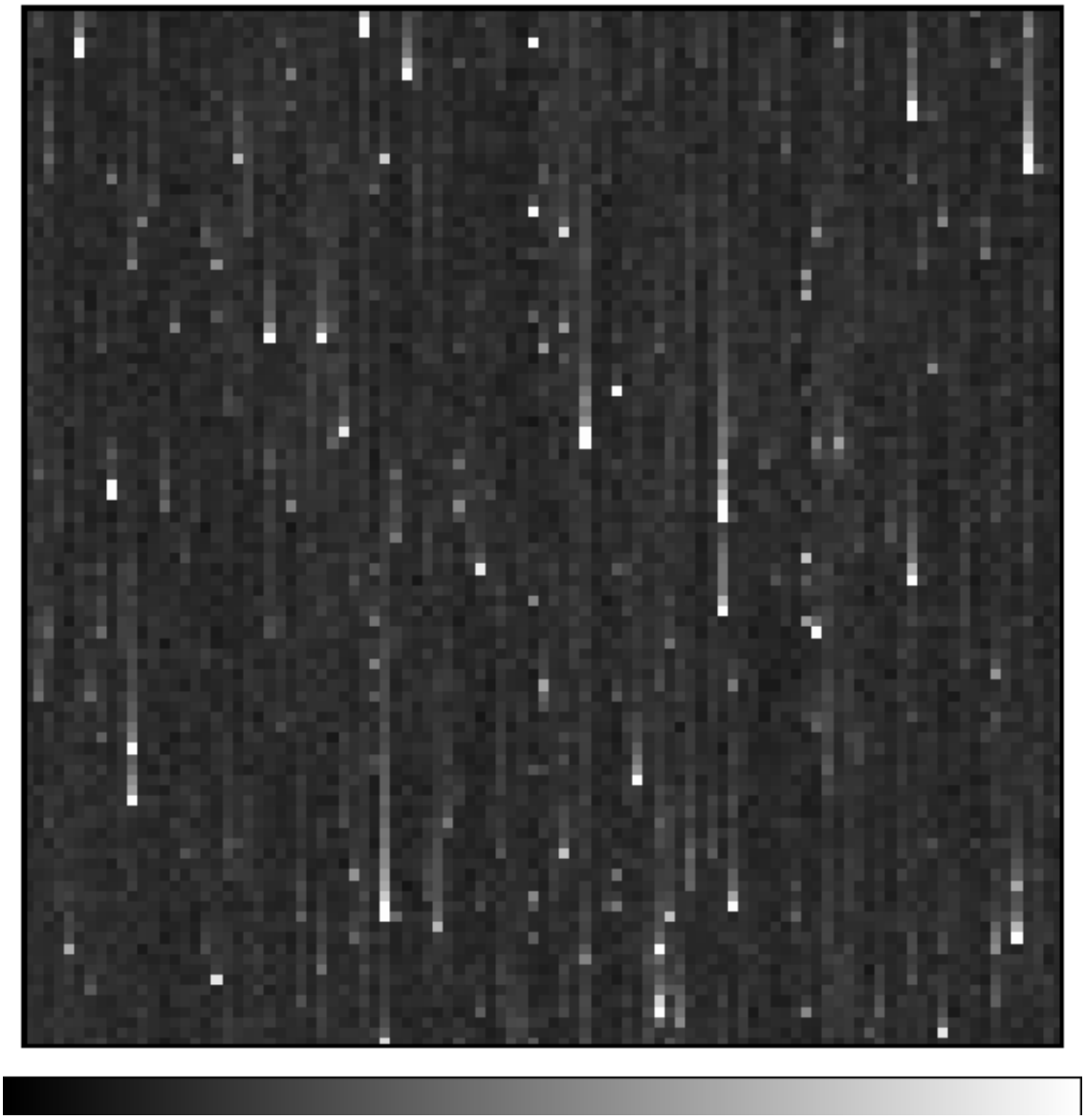

Figure 5. Same image as Figure 4, but showing the region farthest from the read-out amplifier. Most of the brighter hot pixels show vertical trails. There are also faint trails visible without an obvious associated hot pixel – these may be trails from bright cosmic rays where the cosmic ray itself was successfully rejecting in stacking, but some of the trail remains. The image is 100 pixels on a side, and the brightness scale runs from -100 to 1000 counts.

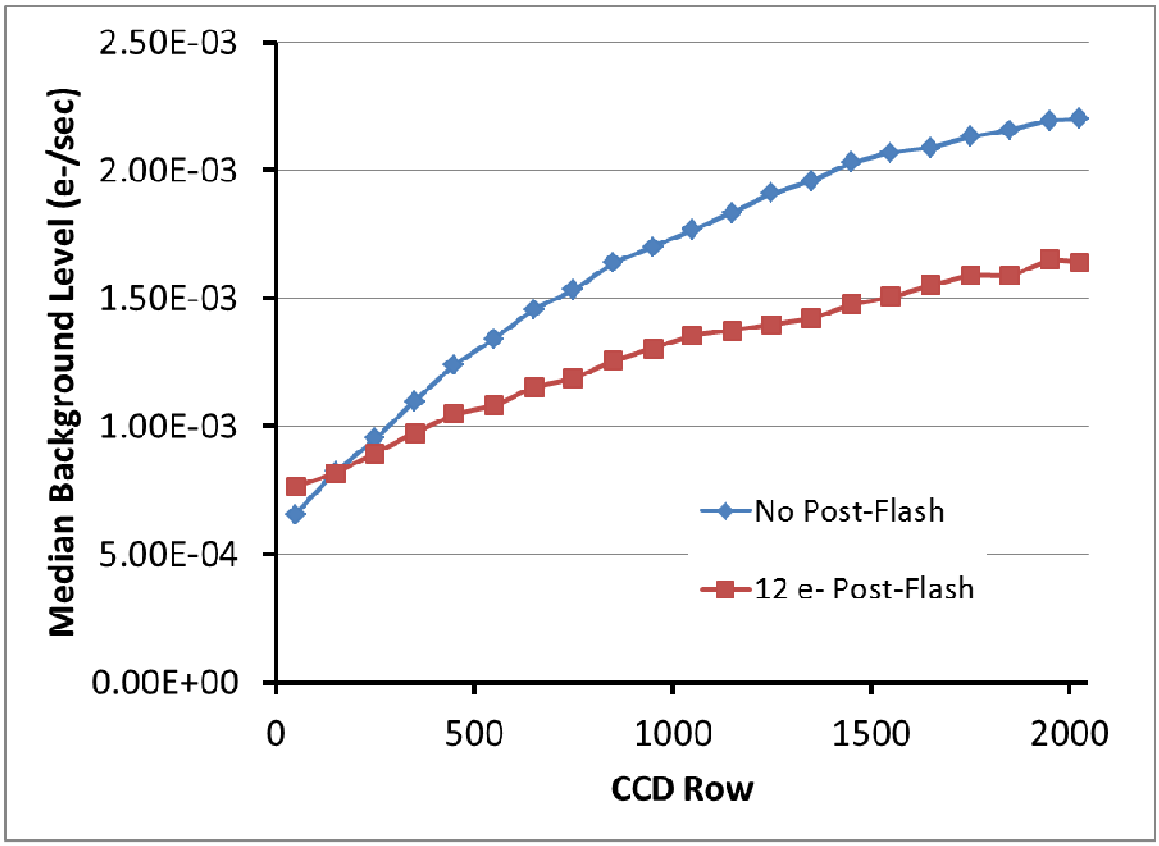

Figure 6. Median background level for averaged stacks of dark frames. The blue values are 76 un-flashed dark frames taken between the Oct. 11 and Nov. 8, 2012 anneals (same image shown in Figure 4 and Figure 5). The red values are 60 dark frames with 12 e- post-flash taken between the Nov. 8 and Dec. 6, 2012 anneals (same image as shown in Figure 14 and Figure 15). This is for the C amplifier quadrant.

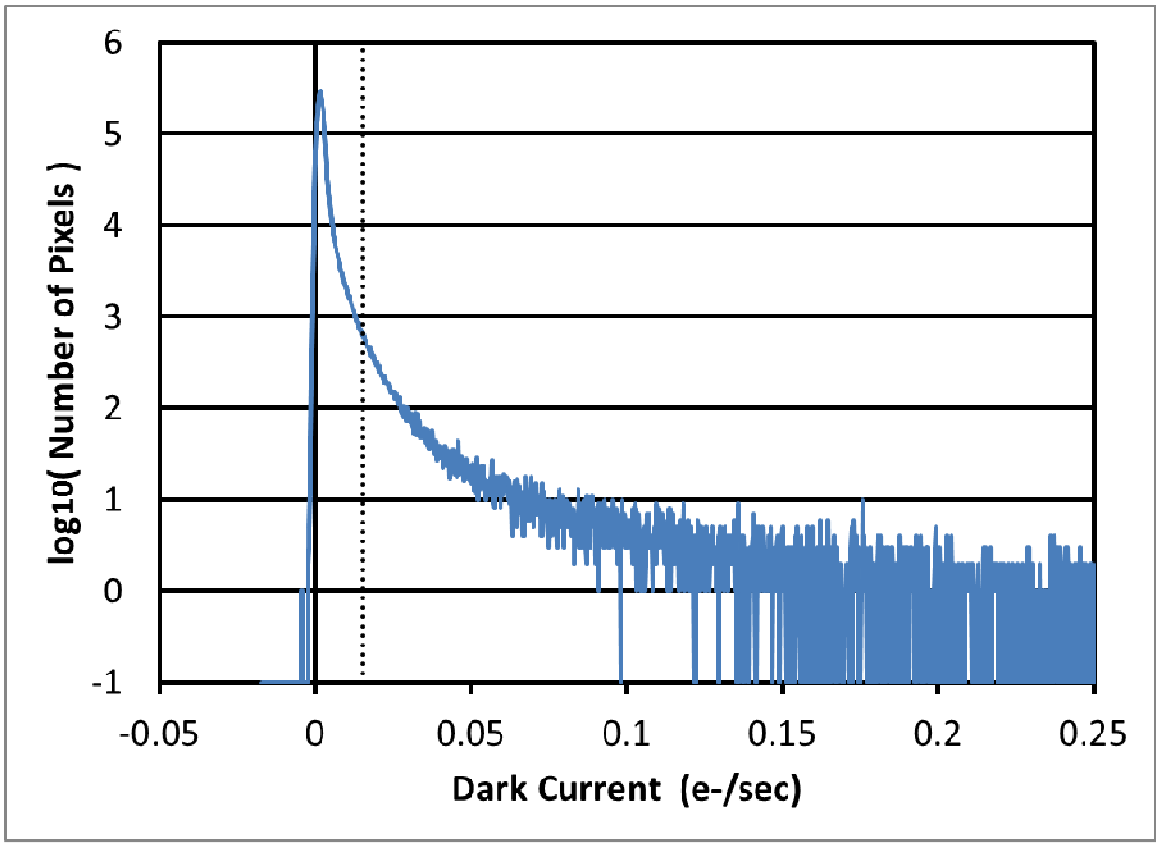

Figure 7. Histogram of hot pixel values for an averaged stack of 76 dark frames taken between the Oct. 11 and Nov. 8, 2012 anneals (similar to image shown in Figure 4 and Figure 5). The vertical dotted line indicates the lower limit of 0.015 e-/sec, below which pixels are set to a constant value in the dark reference files. This is for the C amplifier quadrant, with a 2-pixel border omitted on all sides. The bins on the horizontal axis are 0.1 count in the averaged dark frame, or 0.000173 e-/sec wide. A magnified plot of the region near zero dark current is shown later in Figure 16.

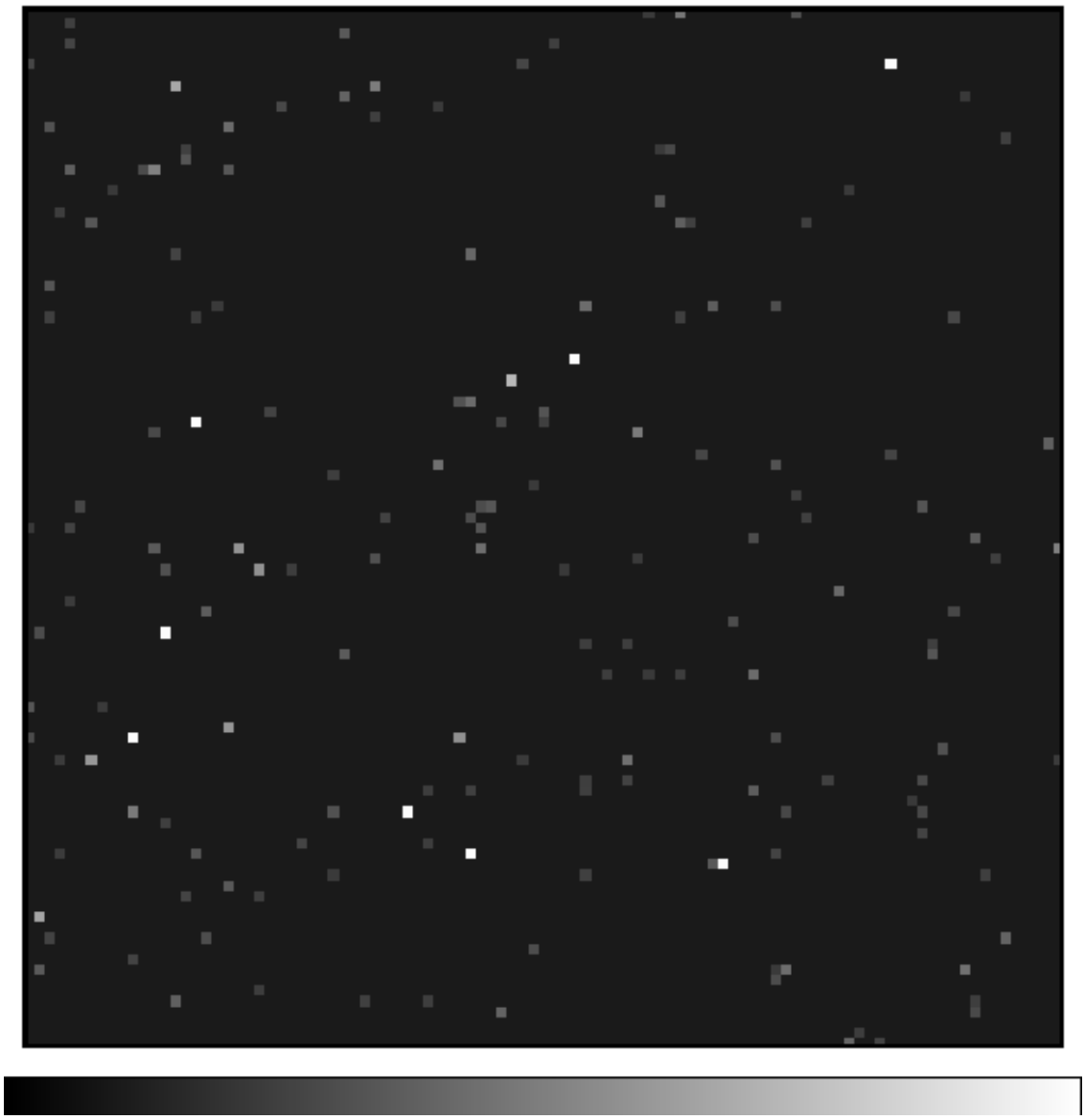

Figure 8. Region of dark reference file nearest the readout amplifier in quadrant C. This is reference file wb81559ri_drk.fits which is appropriate for data taken between Oct. 11 and Oct. 17, 2012. Hot pixels of various brightness are visible, while pixels below 0.015 e-/sec have been set to the median background level of 0.0017 e-/sec. This reference file contains data shown in Figure 2 and Figure 4 and can be compared with those images. The image is 100 pixels on a side, and the brightness scale runs from -0.01 to 0.10 e-/sec.

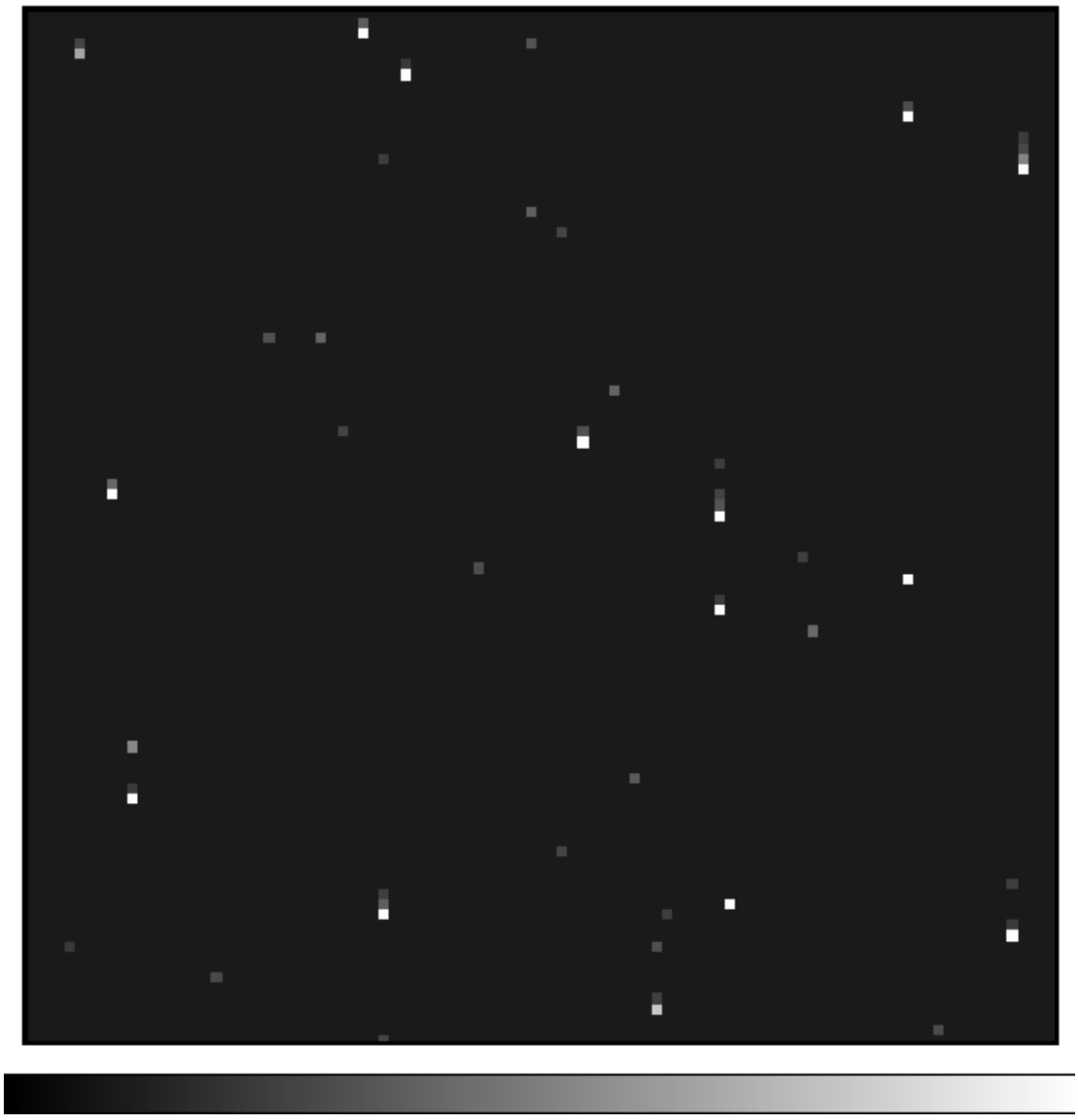

Figure 9. Same dark reference file as Figure 8, but showing the region farthest the readout amplifier. This is similar to Figure 8, but many fewer hot pixels appear due to CTE effects. This reference file contains data shown in Figure 3 and Figure 5 and can be compared with those images. The image is 100 pixels on a side, and the brightness scale runs from -0.01 to 0.10 e-/sec.

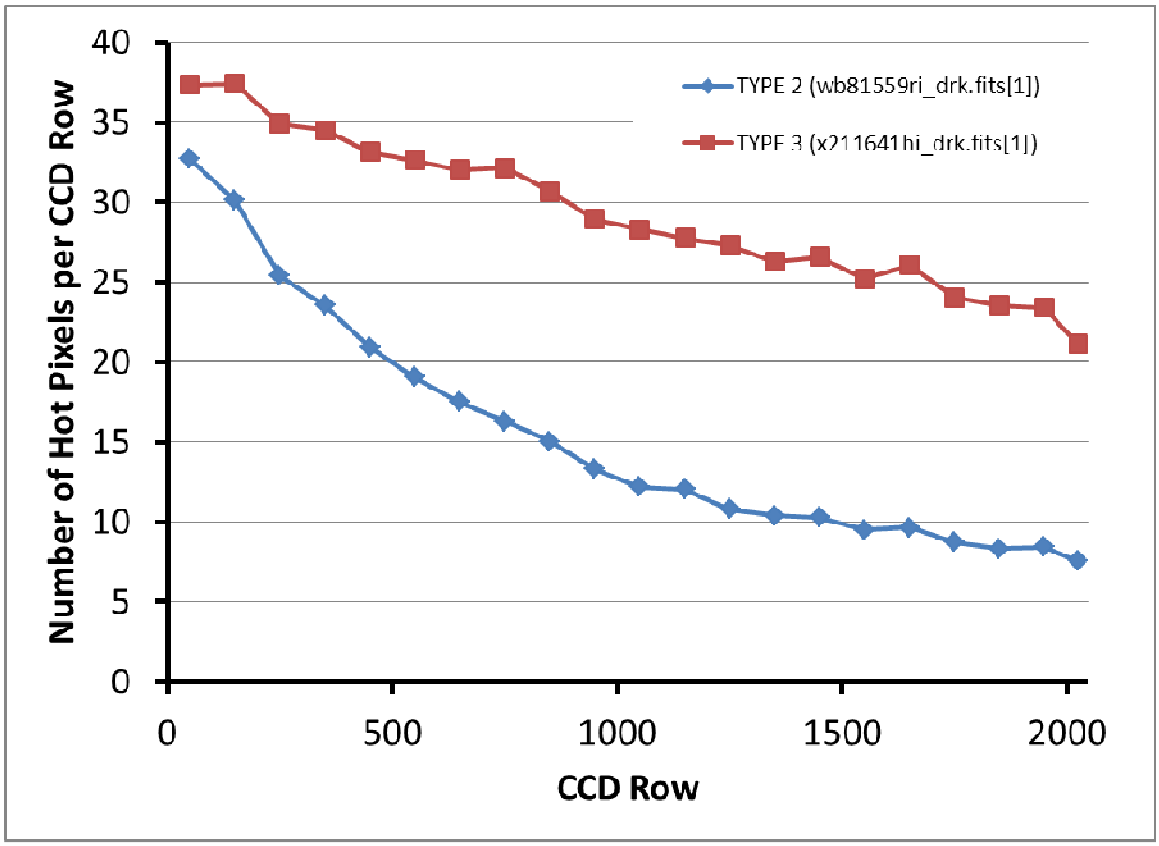

Figure 10. Number of hot pixels per CCD row in the C amplifier quadrant for two representative dark reference files. For the Type 2 reference file (no post-flash) the number of hot pixels per row drops from ~33 near the CCD amplifiers to ~8 at high row numbers. This decrease is caused by CTE effects. For the Type 3 files (with post-flash) the decrease is reduced but still significant. The reference files are from Oct. and Nov. 2012, respectively, and both follow closely after a CCD anneal, so differences due to long-term and short-term evolution are minimized.

Differences Between Type 1 and Type 2 Dark Reference Files

We compared the results of the Type 1 and Type 2 procedures by generating a number of dark reference files using both methods, and then subtracting the reference files from the two methods and studying the residuals. For the vast majority of pixels the two methods gave identical values. However there were typically 100 to 200 pixels spread throughout the field of view where the difference was non-zero. This amounts to only ~0.0009% of the pixels being different between the two methods. These pixels can be understood as follows. Both methods use dark frames taken over a 4-day period, and average these, to produce a dark

reference file for that 4-day period. Hence we would generally expect the dark frames to be identical. However, the initial identification of cosmic rays is performed using all the available datasets. For the Type 1 processing this means all the dark frames taken between two anneals, whereas for Type 2 processing only the dark frames since the prior anneal are used. For a given pixel, the statistical properties across all the available images are used determine whether it is a cosmic ray, and hence the outcome can depend which specific images are processed together. This will in turn affect the averaged pixel value in the dark reference file, and produce different values for the Type 1 and Type 2 processing.

For example, some of the pixels we investigated were near the 0.015 e-/sec cutoff for being included in the reference file as hot pixel. Here rejection of one input pixel due to a cosmic ray would be enough to cause a hot pixel to appear in the Type 1 processing but not the Type 2 processing, or vice versa. Other pixels we investigated underwent large and random variations during the anneal cycle, which caused difficulties with the cosmic ray identification algorithm. For example, Figure 11 gives the values for one such hot pixel where Type 1 and Type 2 processing gave different results. The high brightness of this pixel (comparable to a cosmic ray), together with its extreme variability, present a challenge for the cosmic ray identification algorithm. These differences between the Type 1 and Type 2 processing do not necessarily represent a problem with the new Type 2 processing, but rather are pixels where algorithms do not work well, and the resulting reference file value is not well defined. Again, the number of these pixels is relatively small – roughly 100 to 200 across the field of view.

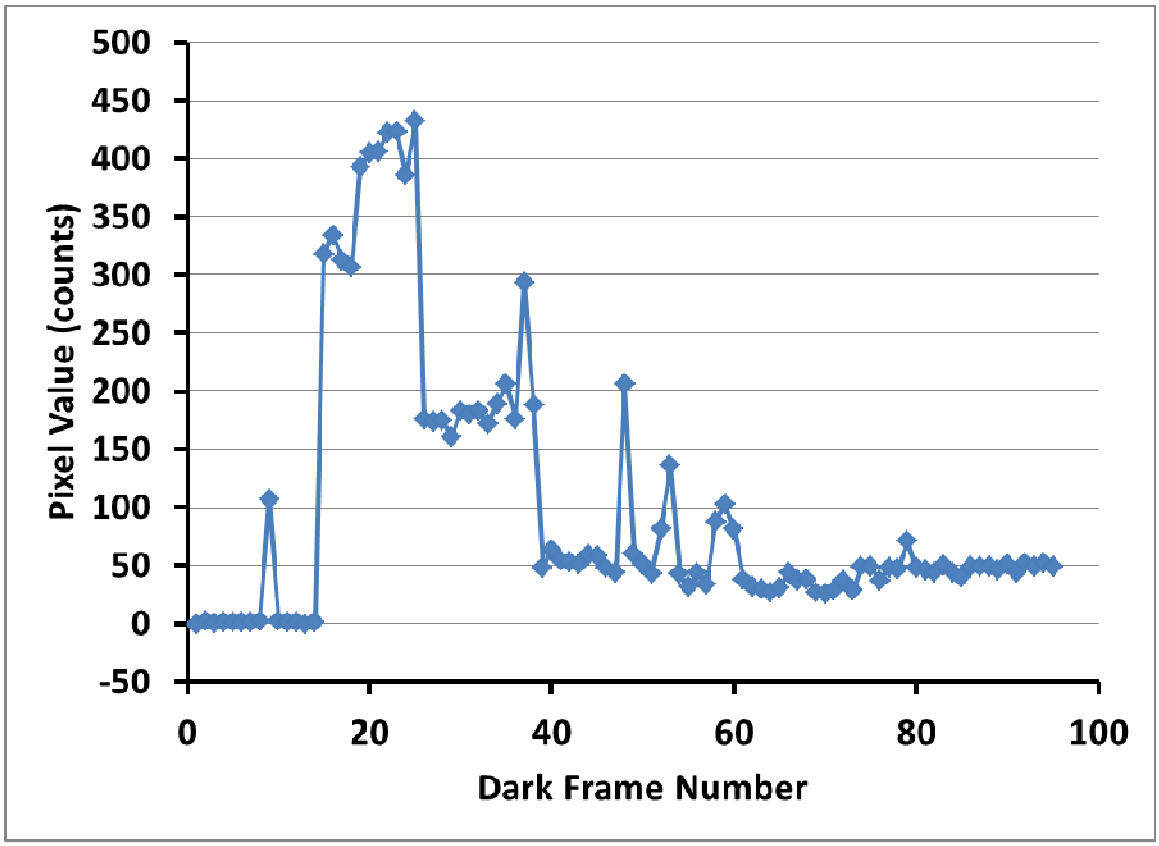

Figure 11. Values of pixel at [1][763,648] in 95 dark frames taken between the Feb. 29 and Mar. 28, 2012 anneals. This pixel is an example where the Type 1 and Type 2 processing give different results. This is caused by Type 1 processing using all 95 frames, whereas the Type 2 processing uses only dark frames taken early in the anneal cycle. Pixels with such complex behavior are rare.

Type 3 Dark Frames and Reference Files

The Type 3 reference files are designed to be as similar as possible to the Type 1 and 2 reference files, but use dark frames with a 12 e- post-flash instead of no post-flash. The motivation here is to reduce CTE loses, and provide image background levels which are more similar to the majority of science images.

Figure 12 and Figure 13 show details of a 900s post-flashed dark frame for regions near and far from the CCD amplifier, respectively. The light contributed by the post-flash has been subtracted via normal pipeline calibration (Biretta and Baggett 2013). These images are taken about one month after the un-flashed images in Figure 2 and Figure 3, and can be directly compared with those. Comparison of the regions near the amplifier without and with post-flash (Figure 2 and Figure 12) show they are very similar. The cosmic ray hits are of course different, but many of the hot pixels appear similar in both images. The post-flashed image

has slightly higher noise, as expected due to the Poisson noise associated with the post-flash light. Comparisons of regions far from the readout amplifier without and with post-flash (Figure 3 and Figure 13) show general similarities, but with subtle differences. Both the images without and with post-flash show significant trailing of cosmic rays and hot pixels due to CTE effects, but in the latter case the trails are generally weaker and shorter. There are also more faint hot pixels visible in the image with post-flash.

Stacking large numbers of frames to remove cosmic rays and reduce noise effects makes the advantages of post-flash more clear. Figure 14 and Figure 15 show a summed stack of 60 post-flashed dark frames taken between the Nov. 8 and Dec. 6, 2012 anneals for regions nearest and farther from the read-out amplifier, respectively. The cosmic rays have been removed and only warm and hot pixels remain. For the region near the amplifier, the images without and with post-flash (Figure 4 and Figure 14) are very similar. As expected some hot pixels have appeared or vanished or changed brightness due to the one-month interval between the images.

The region far from the amplifier shows a dramatic improvement when post-flash is added. Comparison between Figure 5 and Figure 15 shows that many more hot pixels have been preserved and not lost to CTE effects when the post-flash is added. Instead of the image background being dominated by faint trails, the background now is filled with many faint warm pixels.

In the stacked darks with post-flash, the regions near and far from the amplifier (Figure 14 and Figure 15) are much more similar when post-flash is added. The region far from the amplifier has some trailing of the brightest hot pixels, and there are somewhat fewer faint hot pixels, but the general impression is that the images are similar, whereas the images without post-flash appeared very different near and far from the amplifier (Figure 4 and Figure 5).

For the stacked darks without post-flash, we previously saw that the background dark current was much higher in the region far from the amplifier (comparison of Figure 4 and Figure 5, also Figure 6) due to CTE trailing of hot pixels and cosmic rays. The 12 e- post-flash has greatly reduced this effect, but not completely eliminated it. The background in Figure 15 appears higher than that of Figure 14, and this is confirmed by the red values in Figure 6. The median value of background increases from ~0.0008 e-/sec near the amplifier to ~0.0016 e-/sec far from the amplifier.

Figure 16 shows a histogram of hot pixel values for the image shown in Figure 14 and Figure 15 (red line). For comparison purposes the histogram for the un-flashed data is included (blue line, from Figure 7). The distribution for the post-flashed darks (red line) is generally similar to the un-flashed darks used in Type 2 processing (blue line), but at any given count rate there

are about twice as many hot pixels in the post-flashed dark frames. This is, of course, due to CTE losses in the un-flashed darks, and echoes the trend seen in Figure 10.

Figure 17 shows an enlargement of the histogram for the region near zero dark current. The peak of the distribution occurs at a slightly higher dark current for the un-flashed data, and we attribute this to a higher background due to trailing of many hot pixels (as well as cosmic rays). This was discussed in the previous paragraph and is illustrated in Figure 6. The peak of the distribution is slightly wider for the post-flashed data, and this is quantitatively consistent with higher noise due to fewer frames averaged (60 frames for post-flashed data vs. 76 for un-flashed data) and extra photon noise contributed by the post-flash.

The histogram for the post-flashed data also shows a significant population of pixels with negative count rates. These are pixels where the charge associated with the post-flash becomes trapped during readout of the dark frames. This leads to a reduced count level (or sometimes zero count level) in these pixels, which then becomes negative when the post-flash reference file is subtracted during calibration.[12] Approximately 0.2% of the pixels have negative values significantly below the noise tail (defined as <-0.003 e-/sec in Figure 17).

Figure 18 and Figure 19 show enlarged regions of a Type 3 dark reference file (with post-flash). This is reference file x211641hi_drk.fits, which is contemporaneous with the images shown in Figure 12 through Figure 15, and can be compared with those. This reference file was generated using Type 3 processing, and contains 17 input dark frames. Both images show numerous hot pixels, while pixels below 0.015 e-/sec have been set to the median background level of 0.0014 e-/sec. The region far from the readout amplifier shows somewhat fewer hot pixels than the region near the amplifier, but the images are generally similar. The brightest hot pixels in the region far from the amplifier often show short trails one or two pixels in length.

Figure 10, shown earlier, quantifies the number of hot pixels per row as a function of row number, and shows that the un-flash Type 2 reference files lost nearly three-quarters of their hot pixels in regions far from the amplifier. The situation is greatly improved for the post-flashed Type 3 reference file (red values in Figure 10). While there is still significant loss of hot pixels, the fraction lost far from the amplifier is reduced from ~75% to ~43%. Though loss of hot pixels is still not ideal, perhaps a more important consideration is that the hot pixel losses are now much more similar to those expected in typical science images. Perfect preservation of hot pixels is not necessarily the goal here – instead the losses in the dark frames should ideally be as similar as possible to the losses in science images.

[12] The post-flash reference file is built from highly-exposed images, and therefore does not display low count rate pixels due to trapping at low charge levels. See Biretta and Baggett 2013.

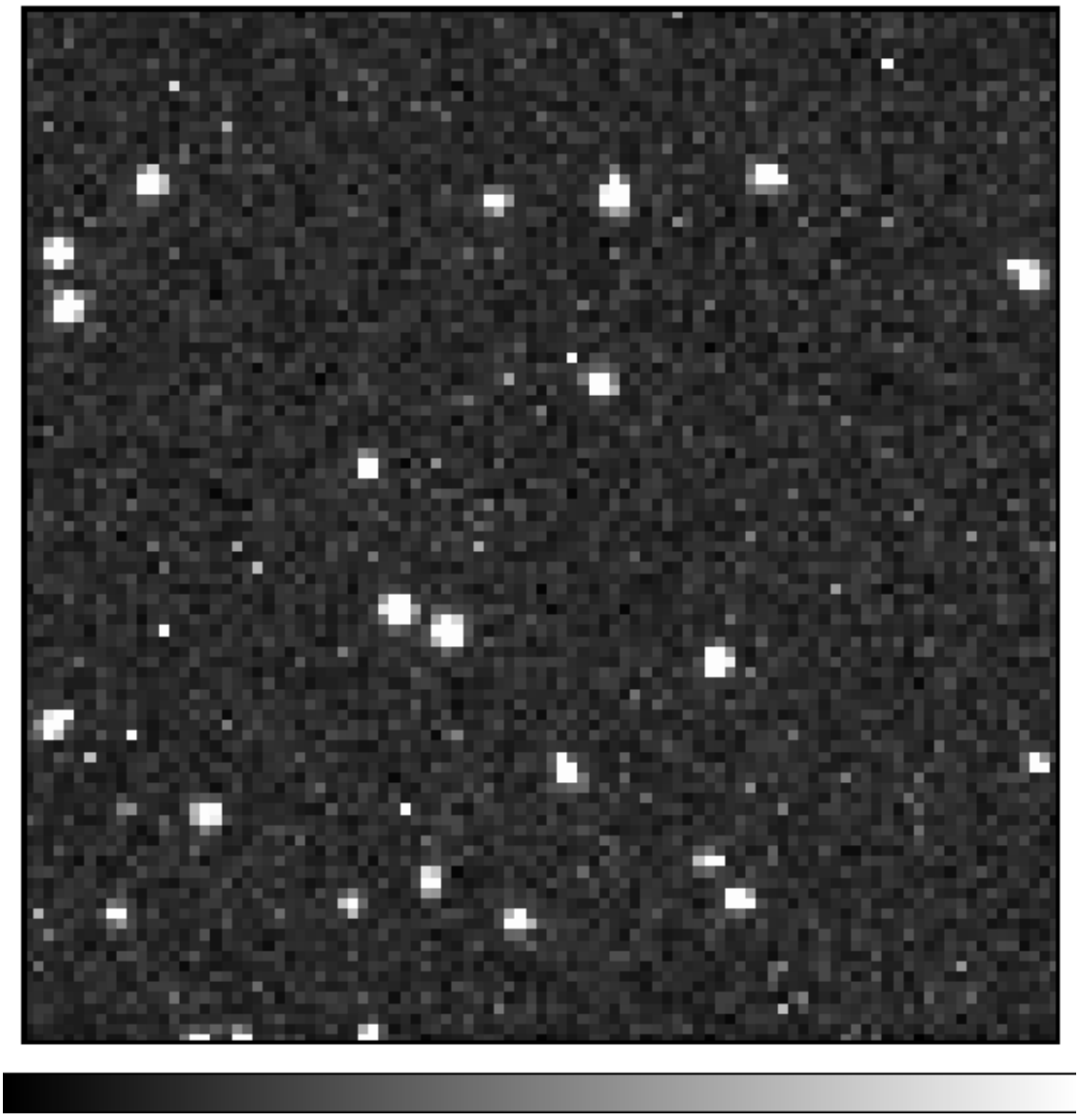

Figure 12. Region nearest the readout amplifier of a typical calibrated 900s dark frame with a 12 e- post-flash in the C detector quadrant (file ic5la4x0q.fits taken on Nov. 8, 2012). Multi-pixel features are cosmic rays, while single pixel features are hot pixels. The image is 100 pixels on a side, and the brightness scale runs from -10 to 50 counts.

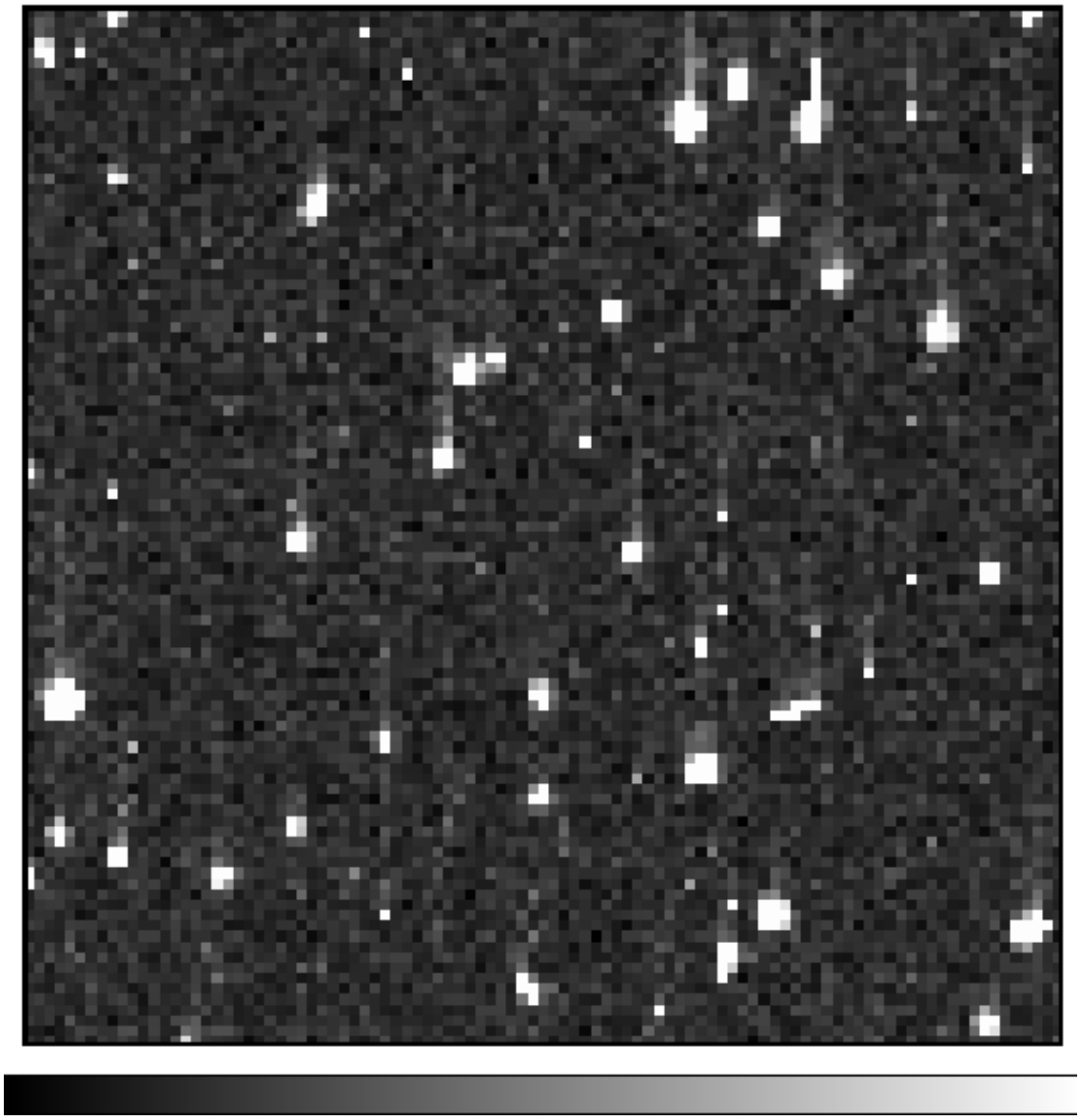

Figure 13. Same image as Figure 12, but showing the region farthest from the readout amplifier. Multi-pixel features are cosmic rays, while single pixel features are hot pixels. Features are trailed vertically due to CTE issues. The image is 100 pixels on a side, and the brightness scale runs from -10 to 50 counts.

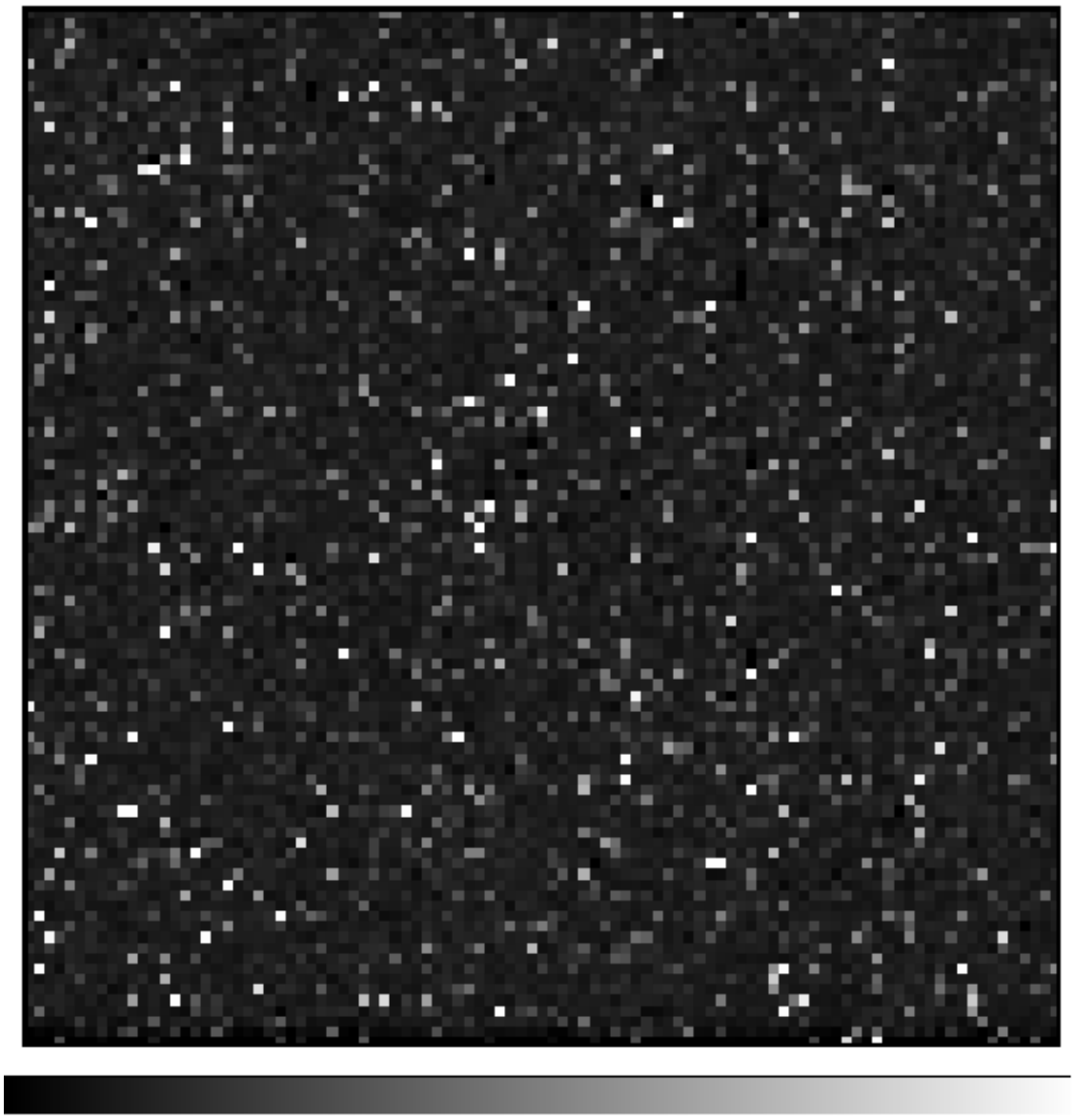

Figure 14. Region near the read-out amplifier of the C quadrant for a summed stack of 60 dark frames with 12 e- post-flash taken between the Nov. 8 and Dec. 6, 2012 anneals. Virtually all the visible features are hot and warm pixels. Small numbers of negative (dark) pixels are also present. The image is 100 pixels on a side, and the brightness scale runs from -100 to 1000 counts.

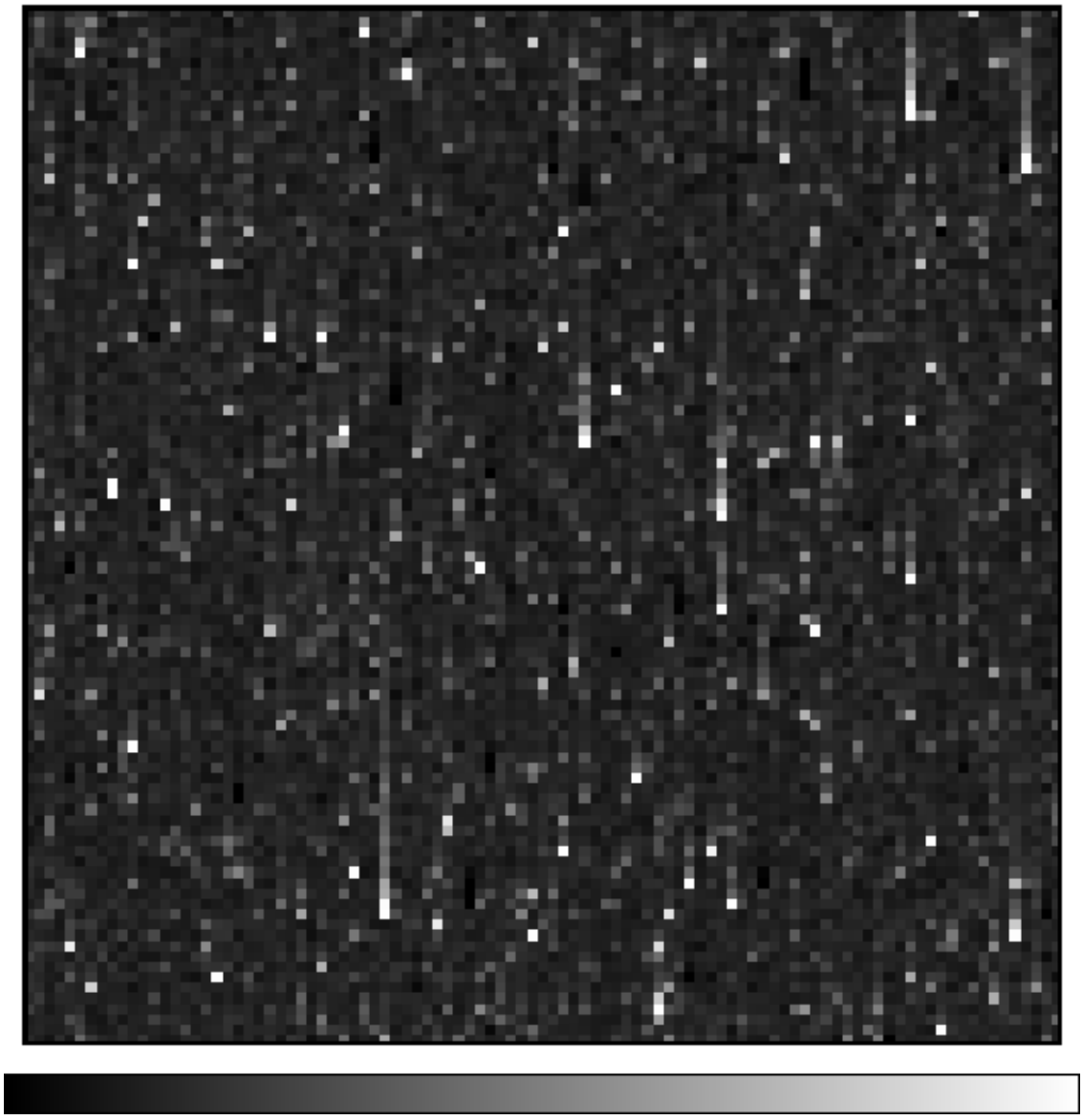

Figure 15. Same image as Figure 12, but showing the region farthest from the read-out amplifier. The brightest hot pixels show vertical trails due to CTE effects. Again small numbers of negative (dark) pixels are present. The image is 100 pixels on a side, and the brightness scale runs from -100 to 1000 counts.

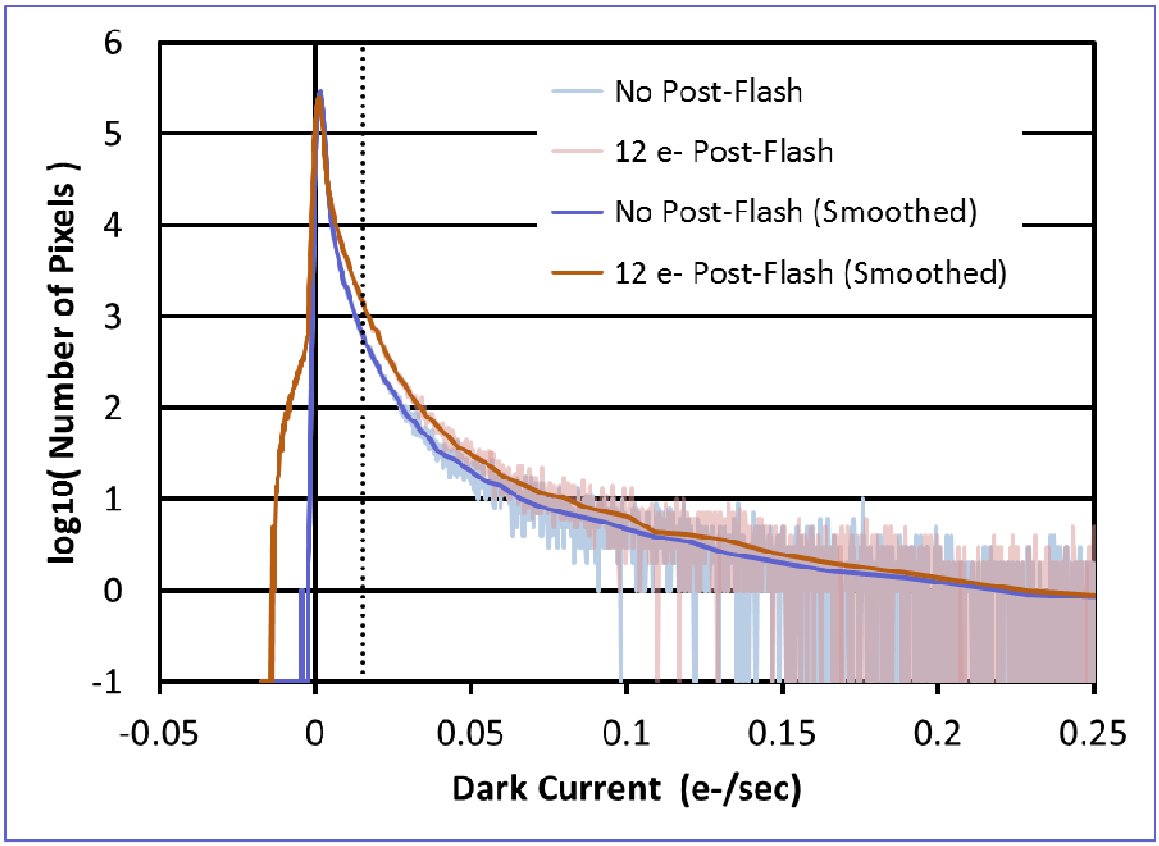

Figure 16. Histogram of hot pixel values for 60 calibrated and averaged 900s dark frames with 12 e- post-flash (red lines). For comparison we include values for 76 averaged dark frames with no post-flash (blue lines, see Figure 7). Light color lines indicate the raw histogram, while darker lines have adaptive smoothing applied to reduce noise. The vertical dotted line indicates the lower limit of 0.015 e-/sec, below which pixels are set to a constant value in the dark reference files. This is for the C amplifier quadrant, with a 2-pixel border omitted on all sides. The bins on the horizontal axis are 0.1 count in the averaged dark frame, or 0.000173 e-/sec wide.

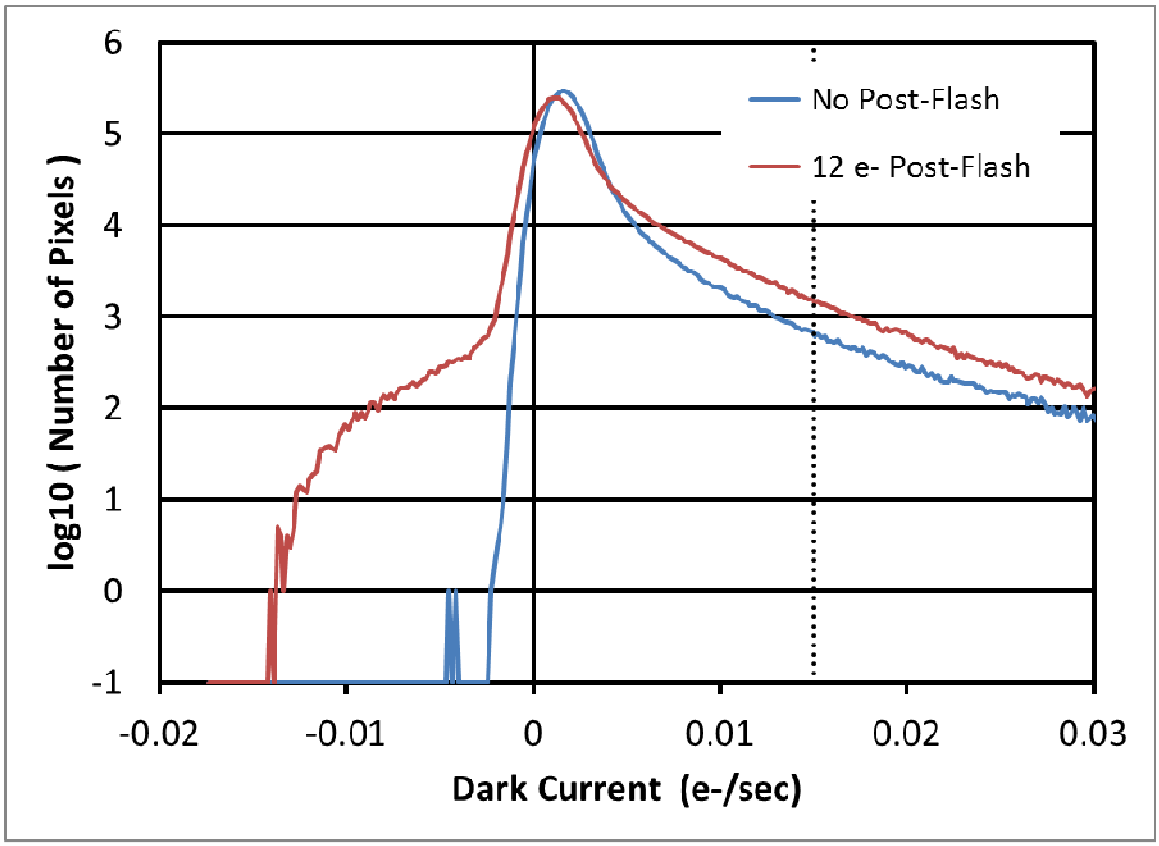

Figure 17. Enlargement of the region near zero dark current for the histogram in Figure 16.

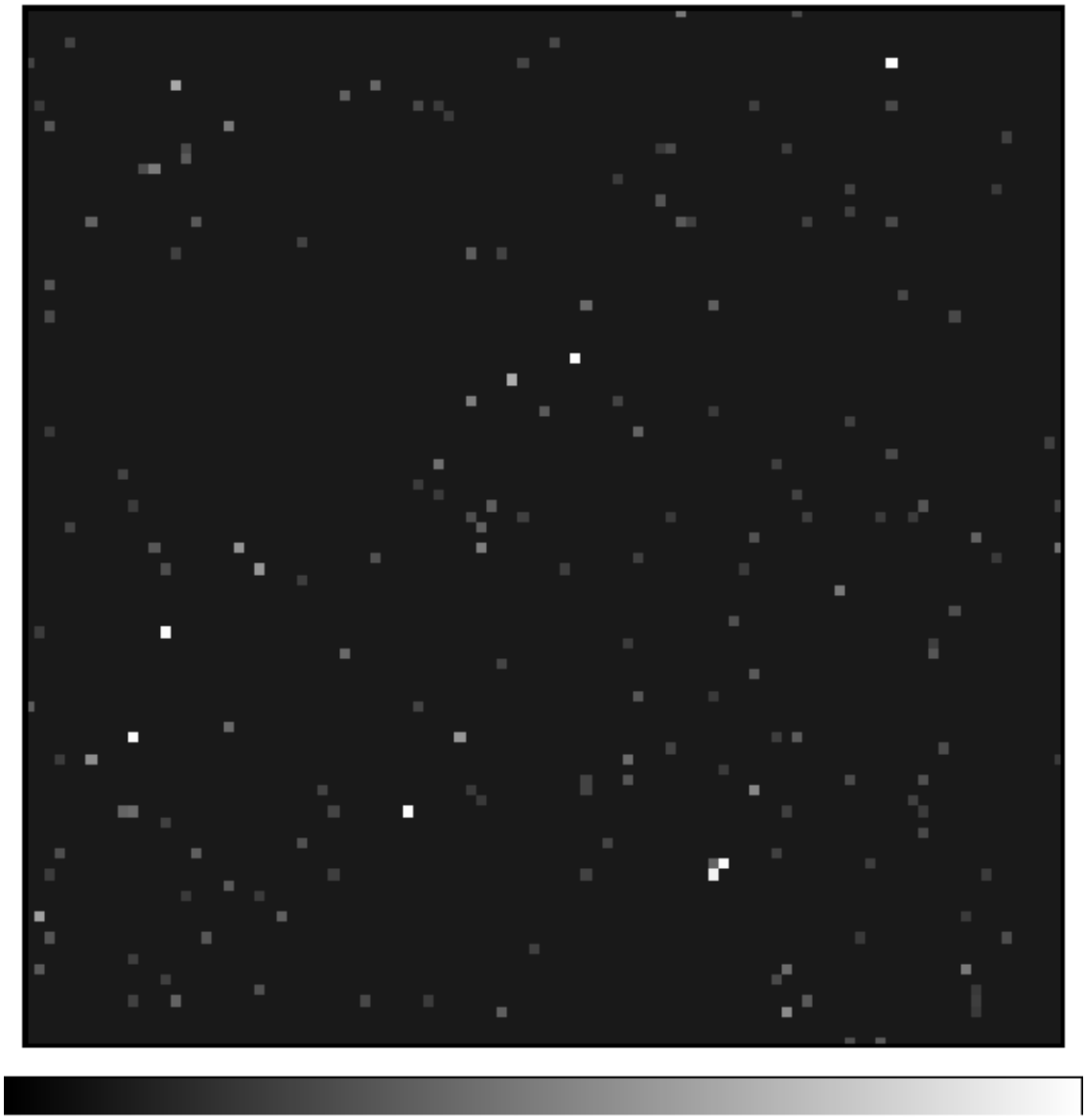

Figure 18. Region nearest the readout amplifier in quadrant C for a typical Type 3 dark reference file. This is reference file x211641hi_drk.fits which is appropriate for data taken between Nov. 8 and 12, 2012. Hot pixels of various brightness are visible, while pixels below 0.015 e-/sec have been set to the median background level of 0.0014 e-/sec. This reference file contains data shown in Figure 12 and Figure 14 and can be compared with those images. The image is 100 pixels on a side, and the brightness scale runs from -0.01 to 0.10 e-/sec.

Figure 19. Same dark reference as Figure 18, but showing the region farthest from the readout amplifier. Hot pixels of various brightness are visible, while pixels below 0.015 e-/sec have been set to the median background level of 0.0014 e-/sec. This reference file contains data shown in Figure 13 and Figure 15 and can be compared with those images. The image is 100 pixels on a side, and the brightness scale runs from -0.01 to 0.10 e-/sec.

Long-Term Evolution

Plots showing the long-term evolution of the median dark current and hot pixel population are made as part of the routine processing during generation of dark reference files. These plots serve as a check for bad dark frames and instrumental anomalies.

Figure 20 and Figure 21 show a typical set of plots for the median dark current. These show the median dark current as a function of epoch during the entire lifetime of WFC3. Each data point represents a single 900 sec dark frame. The median dark current is computed by calculating the median counts per pixel over the image (excluding pixels flagged as cosmic rays and hot pixels) and then scaling by the exposure time and CCD gain. Figure 20 shows the results for data file extension 1, which contains the C and D amplifier quadrants on chip 2, and Figure 21 is for data file extension 4, which contains the A and B amplifier quadrants on chip 1. The horizontal axis shows the days since the initial cool-down of the WFC3 detectors to their operating temperature on June 11, 2009, and the vertical axis shows the median dark current in e-/hour. Vertical red (dark) lines indicate the dates of CCD anneal procedures, and the cyan (light) vertical lines indicate the dates of HST computer failures.

As we can see in Figure 20, the median dark current increases from about 2 e-/hr early in the mission, to about 7 e-/hr by the end of the Type 2 processing (day 1246 or Nov. 8, 2012). The data through this time are generated with Type 1 or Type 2 processing using un-flash dark frames. When the transition to Type 3 processing and post-flashed dark frames occurs at day 1246, the median dark current drops to about 5 e-/hr, and then continues a gradual increase afterwards. This sharp decrease at day 1246 can be understood as a reduction in the CTE trailing due to the addition of the 12 e- post-flash. As previously shown in Figure 6, CTE-related effects will increase the median background of the image due to trailing of hot pixels and cosmic rays, and these effects are significantly reduced in post-flashed data. Hence the long-term evolution of the background dark current is determined by at least two factors – a gradual increase in the intrinsic "background" dark current due to radiation damage to the detector, and also an increase in the background due to many overlapping trails caused by CTE effects. Without further work it is difficult to say which of these effects dominates. But we note that the effects of CTE losses are very significant. According to Figure 6 which is generated from un-flashed data taken in Oct. 2012, the background dark current increases by

a factor ~2.5 between image rows near the amplifier (very little CTE losses) and the center of the CCD (which approximates average CTE losses for the entire CCD). The increase in background dark current seen in Figure 20 over the WFC3 mission up to this time is a factor ~3.5. Hence most of the long-term increase in background dark current can probably be attributed to CTE-related effects, rather than a true increase in the intrinsic background dark current due to radiation damage. [13]

Figure 21 for the A and B amplifier quadrants show very similar effects, although the dark current is slightly lower. The lower dark current is likely due to intrinsic differences between CCD chip 1 and 2, or in the associated electronics.

Figure 22 and Figure 23 show typical plots which monitor the numbers of hot pixels. These plot the percentage of hot pixels in each dark frame vs. the number of days since the initial cool-down of WFC3 to its normal operating temperature. Each data point represents a single 900s dark frame. Here "hot pixel" is defined as exceeding 9 counts in the 900s calibrated dark frame, which corresponds to about 0.0156 e-/sec or 56 e-/hr. Figure 22 is for data file extension 1 (the C and D amplifier quadrants), and Figure 23 is for data file extension 4 (the A and B amplifier quadrants).

The hot pixel plots show a combination of short- and long-term effects. There is a continual rapid growth of "temporary" hot pixels due to cosmic ray hits on the detector, but most of these are removed during the monthly anneal procedure where the CCD detectors are warmed-up for several hours. The rapid growth combined with the monthly anneals causes a short-term saw-tooth pattern in the data. Underlying this pattern is a more gradual long-term growth of "permanent" hot pixels which are not removed by the anneals. The long-term growth ultimately dominates, with a growth from zero to about 1.3% permanent hot pixels by the end of the Type 2 processing in Nov. 2012.

When Type 3 processing starts, which uses dark frames with a 12e- post-flash, we see a sudden jump in the number of permanent hot pixels to ~2.7%, followed by the usual long-term increase. This jump is due to a reduction of CTE losses. As seen earlier in Figure 10, for un-flashed data the majority of hot pixels far from the CCD amplifier are lost to CTE effects during readout; the jump is simply a result of these pixels now reaching the amplifier and being counted.

A better way to track the long-term development of hot pixels might be to look at only the CCD rows nearest the amplifier – this would largely eliminate CTE loss effects and give a

[13] A better test for increases in the intrinsic background dark current would be to plot the median level in only the CCD rows nearest the amplifier. But that is beyond the scope of the current report.

clearer picture of the hot pixel evolution. We have done this in Figure 24. Here we consider only the first 100 rows of the C amplifier quadrant. Each data point represents a single dark reference file, and we have counted the percentage of hot pixels above 0.015 e-/sec. The previously noted short-term pattern is quite apparent – there is rapid growth of "temporary" hot pixels, followed by a sudden reduction after the monthly anneal procedures. The short-term growth rate of temporary hot pixels between anneals is about 0.4% per month; this rate remains approximately constant throughout the WFC3 lifetime. The long-term growth of permanent hot pixels is similar to that in Figure 22 and Figure 23 for the Type 3 post-flashed data. By the end of Cycle 20 there are about 2.2% of permanent hot pixels, or an annual growth rate of about 0.5%. The large jump seen in Figure 22 and Figure 23 when we start using Type 3 (post-flashed) darks has been virtually eliminated -- Figure 24 shows only a slight step up in the number of hot pixels when Type 3 darks begin.

Several instrument anomalies are readily apparent in Figure 24. For reasons that are not entirely clear, the day 1161 (Aug. 15, 2012) anneal procedure was much less successful than other anneals in removing the "temporary" hot pixels. This and other anomalies associated with the Aug. 2012 anneal have been documented by Baggett, et al., 2013. Similarly the day 1554 (Sep. 12, 2013) anneal was not successful in removing the temporary hot pixels. Neither of these anomalous anneals appears to have had significant long-term effects. In both cases a subsequent normal (successful) anneal was able to remove the extra temporary hot pixels and return the percentage of hot pixels to expected levels.

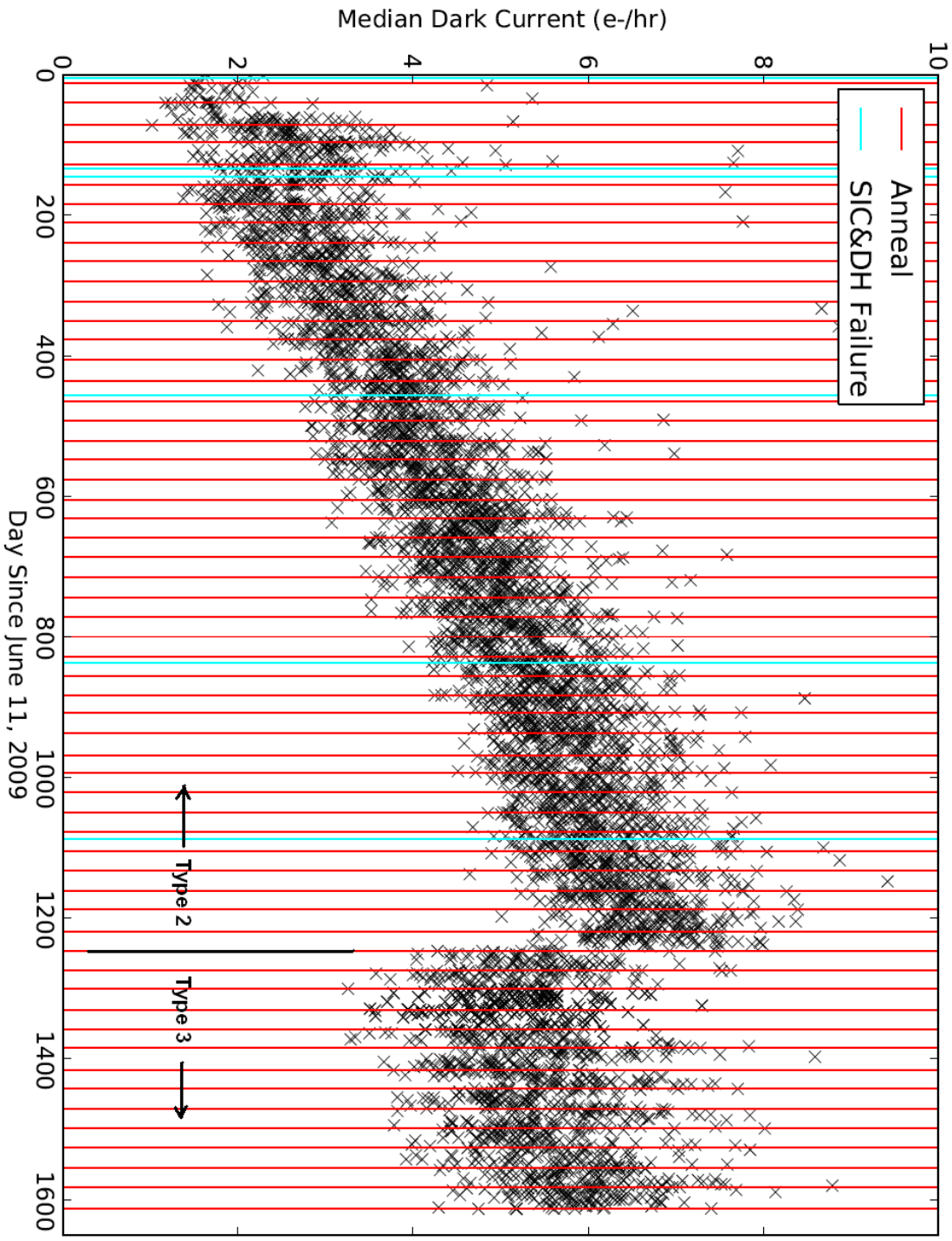

Figure 20. Dark current monitoring plot generated by median_plot.py script. This plots the median dark current for all pixels in the image as a function of days since the initial cool-down of the WFC3 detectors. After day 1246 (Nov. 8, 2012) "Type 3" processing is used with 12 e-/pixel post-flashed dark frames; prior to that date "Type 1" or "Type 2" processing is used with un-flash dark frames. Red (dark) vertical lines indicate times of CCD anneal procedures. Cyan (light) vertical lines indicate times of spacecraft SIC&DH issues. This plot is for the C and D amplifier quadrants (data file extension 1).

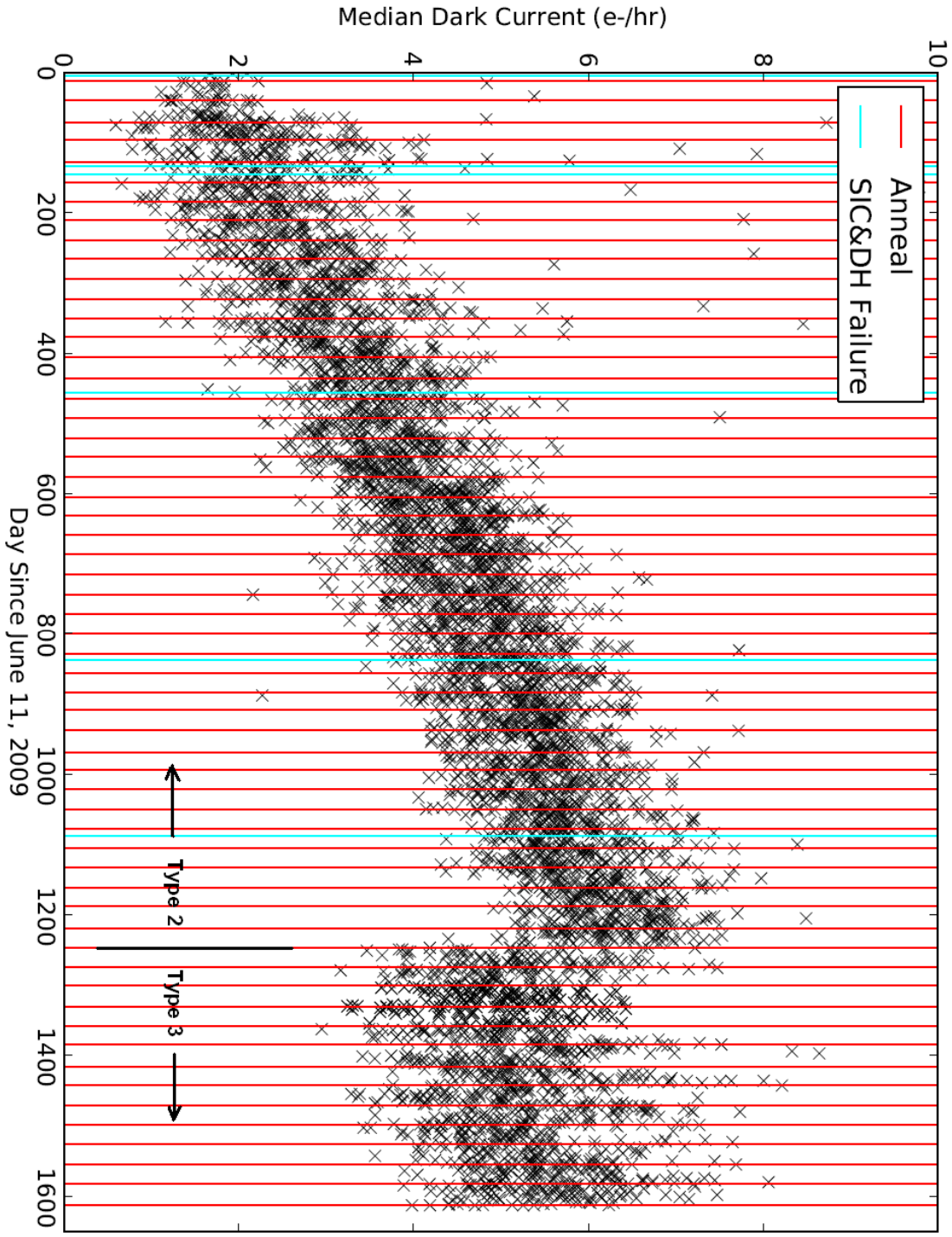

Figure 21. Dark current monitoring plot generated by median_plot.py script. This is the same plot as Figure 20, but for the A and B amplifier quadrants (data file extension 4).

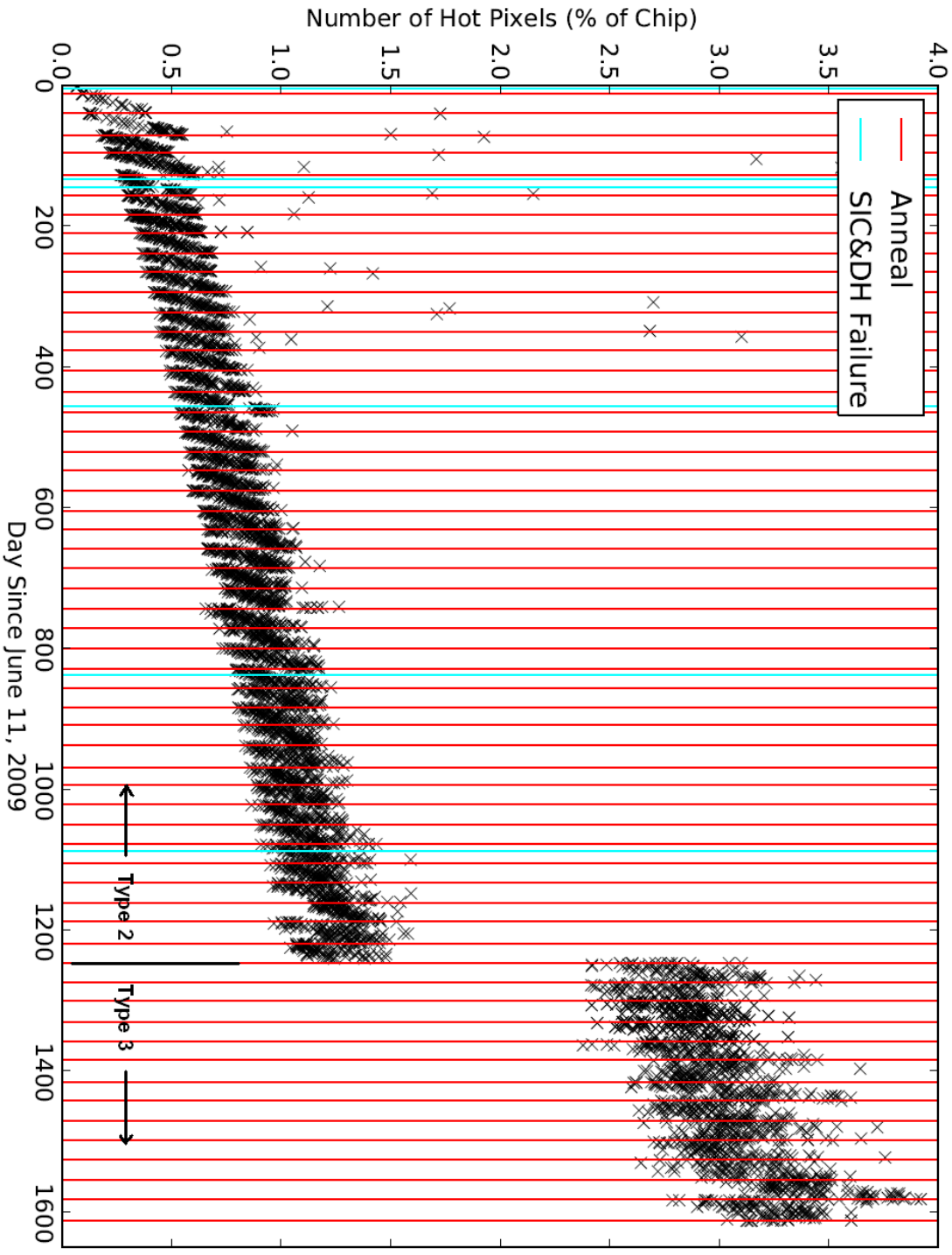

Figure 22. Hot pixel monitoring plot generated by the hotpix_plot.py script. This plots the fraction of hot pixels as a function of days since the initial cool-down of WFC3. After day 1246 (Nov. 8, 2012) "Type 3" processing is used with 12 e-/pixel post-flashed dark frames; prior to that date "Type 1" or "Type 2" processing is used with un-flash dark frames. Red (dark) vertical lines indicate times of CCD anneal procedures. Cyan (light) vertical lines indicate times of spacecraft SIC&DH issues. This plot is for the C and D amplifier quadrants (data file extension 1).

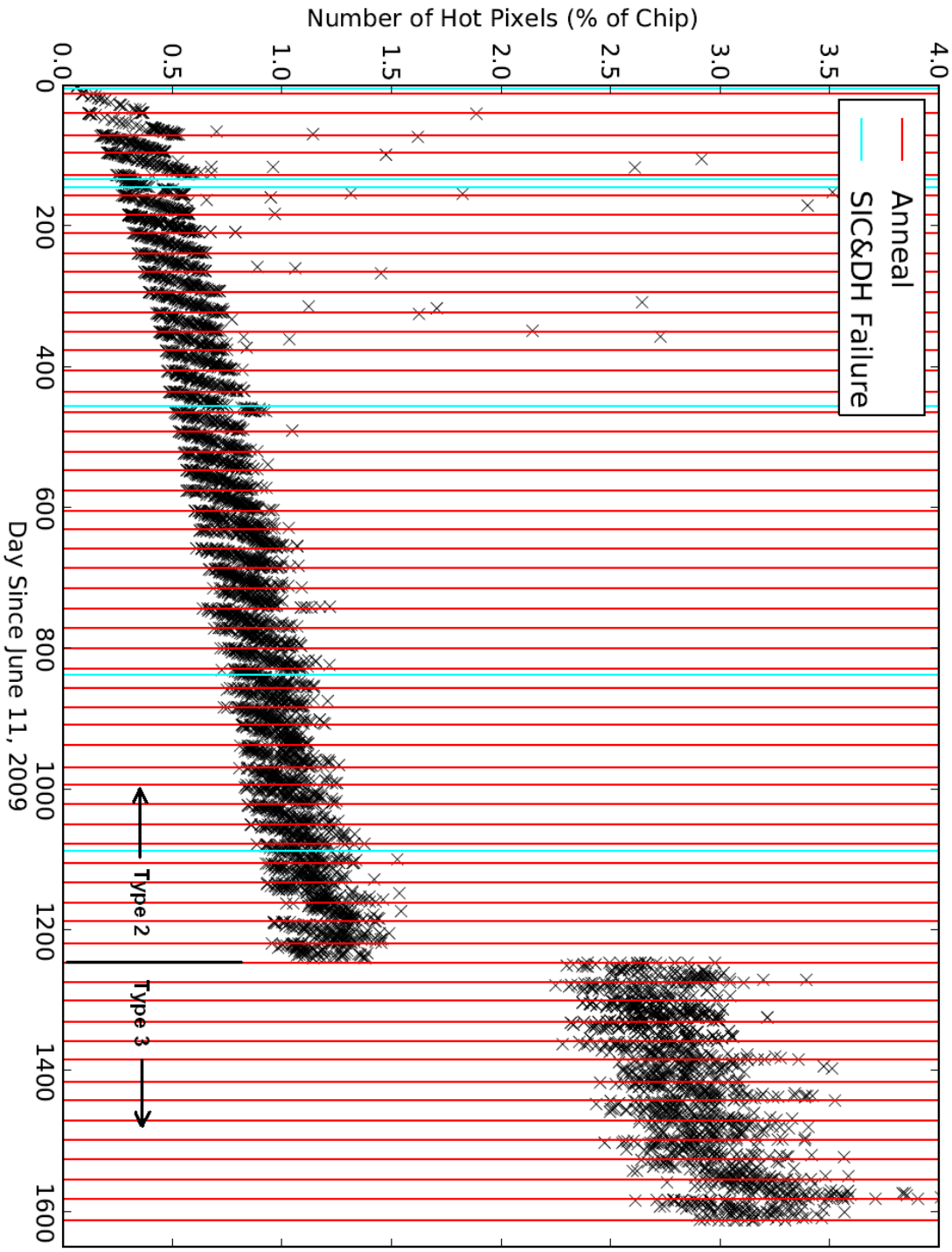

Figure 23. Hot pixel monitoring plot generated by hotpix_plot.py script. This is the same plot as Figure 22, but for the A and B amplifier quadrants (data file extension 4).

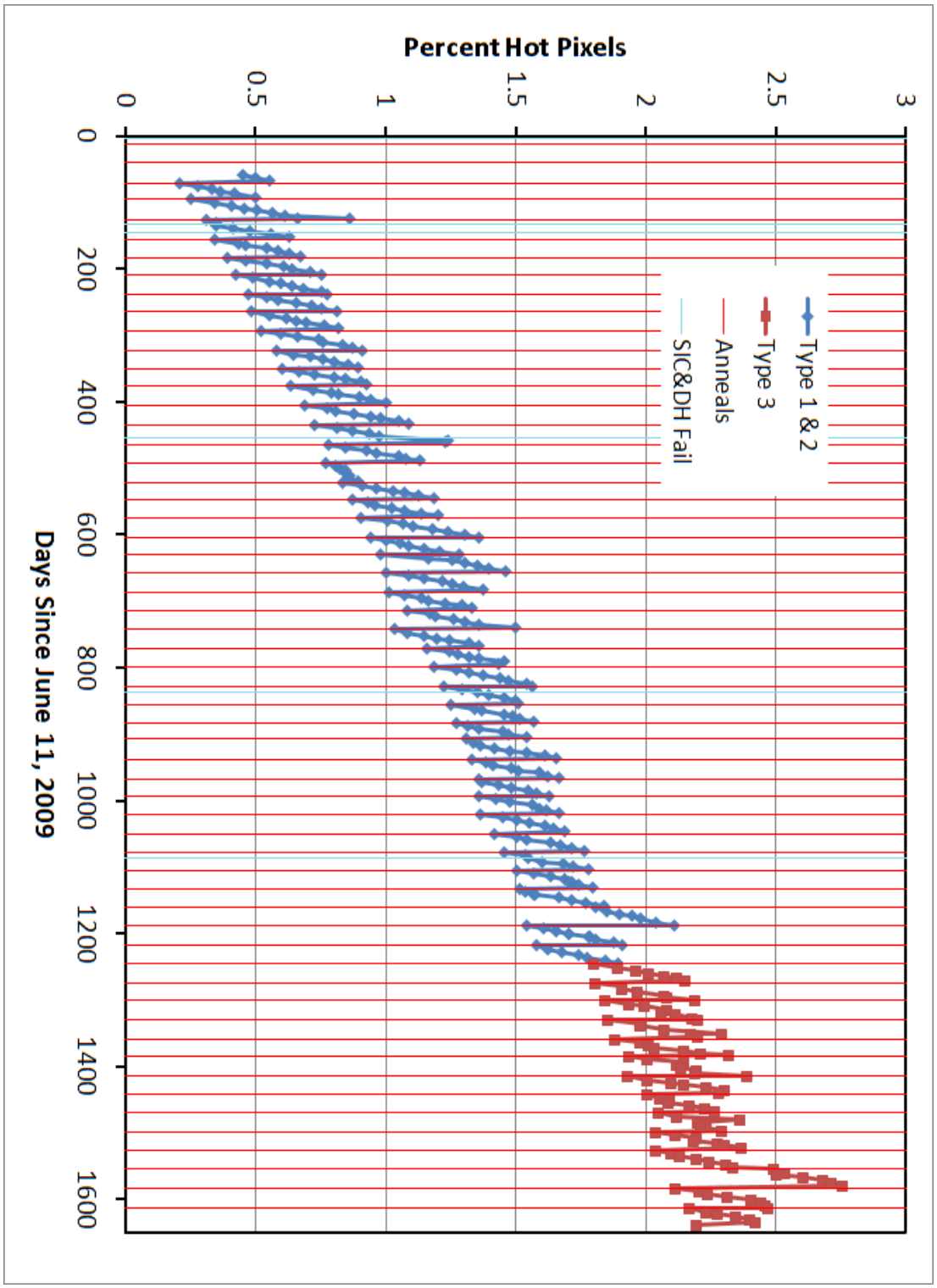

Figure 24. Fraction of hot pixels in the first 100 rows of reference files as a function of days since the initial cool-down of WFC3. After day 1246 (Nov. 8, 2012) "Type 3" processing is used with 12 e-/pixel post-flashed dark frames; prior to that date "Type 1" or "Type 2" processing is used with un-flash dark frames. Red (dark) vertical lines indicate times of CCD anneal procedures. Cyan (light) vertical lines indicate times of spacecraft SIC&DH issues. This plot is for the C amplifier quadrant only.

Reference File Delivery Times

One of the primary motivations in moving from the Type 1 to Type 2 dark reference files was to reduce the time between observation and dark reference file creation and delivery. Figure 25 plots the time between observation and file delivery for all dark reference files since the start of the WFC3 mission. It appears that we have been fairly successful in reducing the reference file delivery times. The Type 1 reference files were delivered for observations prior to Feb. 29, 2012 and during this time the average delivery time was 130 days with a median value of 123 days. The Type 2 reference files were delivered between March 1, 2012 and Nov. 8, 2012 during which the average delivery time was 18 days with a median value of 13 days.

An effort was also made to keep delivery times relatively short for the Type 3 dark reference files. There was some delay in Nov. 2012 to Feb. 2013 while the CCD post-flash was being calibrated and the new Type 3 procedure was being developed, but after March 1, 2013 the delivery times were comparable to those for Type 2 files. After March 1, 2013 the average delivery time for the Type 3 files was 14 days with a median value of 13 days. These delivery times represent a great improvement over those early in the WFC3 mission.

The factors which still limited the delivery times late in Cycle 20 (Apr. to Nov. 2013) were as follows: We generated a new dark reference file for every 4 days of observation, which implied an average wait time of 2 calendar days. Typically 2 – 3 days were required between observations and availability of the data in the HST archive. Processing of the raw dark frames into reference files required about 2 business days, and delivery of the reference file back into the archive (including format and validation tests) required another 1 to 2 business days. And finally we generated dark reference files about once a week, which implied an average delay of about 4 calendar days. These factors sum together to cause a time delay between observation and file delivery of 13 to 15 calendar days, which is roughly the observed delay in late Cycle 20.

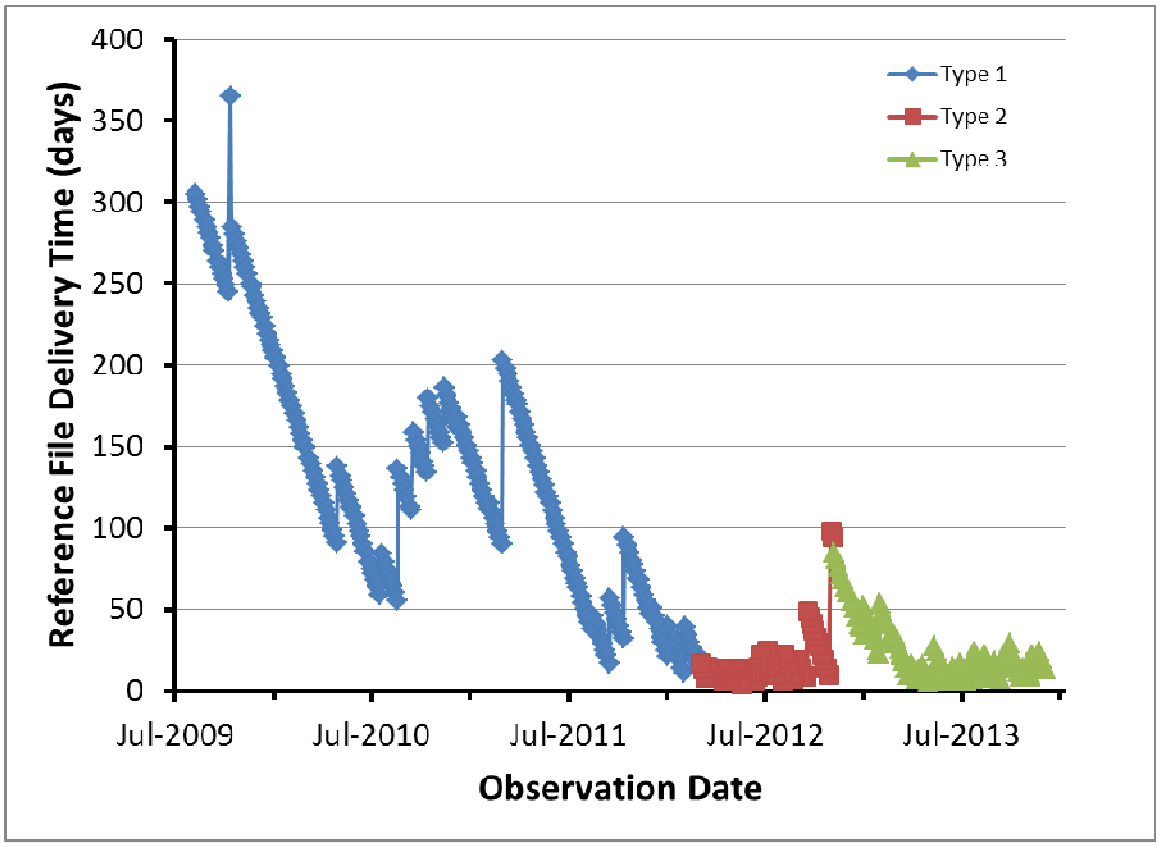

Figure 25. Dark reference file delivery time, defined as the time between observation and file delivery, vs. observation date for all dark reference files since the start of the WFC3 mission. Type 1 files were delivered for data taken prior to Feb. 29, 2012; Type 2 files were delivered for data taken between Feb. 29, 2012 and Nov. 8, 2012; Type 3 files were delivered for data taken after Nov. 8, 2012.

Future Work

There are several areas where improvements should be explored in creating the dark reference files. The first would be automation of the processing which could have two positive impacts – further reduction in the delay between observation and reference file delivery, and a reduction in the manpower required to generate the dark reference files. Late in Cycle 20 the largest single contributor to the delay is that the reference files are generated once per week, and this is is largely determined by the available manpower assigned to the processing (0.2 to 0.3 FTE). Full automation of the processing might allow generation of new reference files

seven days a week without human intervention, which would reduce the average delivery times by about 4 days.[14] Automation should also reduce the time to compute the reference files themselves from ~2 days to a few hours. If the testing and delivery phases could also be automated, an additional 1 to 2 days could be gained.[15] These factors together could reduce the average delivery time to about 6 days. At that point the limiting factors would be the 4-day interval at which new reference files are delivered, and the 2 to 3 day wait for raw data to appear in the HST archive.[16]

We have shown that better statistics can be used to evaluate the long-term evolution of the dark current – for example computing statistics using only CCD rows near the amplifier to reduce the effects of CTE losses. These will be incorporated in future routine processing to generate dark reference files.

While we typically used 10 to 15 raw dark frames to generate each reference file, there are occasions where as few as 4 or 5 raw dark frames are used (c.f. Table 2). This is usually the result of high WFC3 usage by time-critical science observations. Dark calibration observations requested at such times are cancelled in favor of science observations, with the result that few dark frames are taken during the 4-day interval for creating dark reference files. While dark frames can be taken during earth occultation, this is often not possible due to SAA impacts during the occultations. Some attention is probably needed to these events – it may be useful to study what impact this has on the quality of the calibration, and whether the situation can be improved. Cosmic ray rejection at these times is probably not an issue, since dark frames outside the 4-day intervals are typically used by the scripts when identifying cosmic rays. But there may be small image regions where no valid data exist when as few as 4 images are stacked.

It may be worth exploring whether the 0.015 e-/sec threshold for including hot pixels in the reference file should be lowered. Often we have seen that there is a significant population of

[14] Probably we should continue have a scientist review the input raw dark frames and the resulting reference files, but this activity could be performed perhaps once per week and after the reference files are delivered. There might be some hazard of needing to "recall" a bad or sub-standard file that was delivered, but these incidents should be very rare. Statistical checks could be coded into the automated pipeline which might discard bad input files, or prevent delivery of anomalous reference files, and thus provide a first line of defense against delivery of problematic files.

[15] Automation of the file testing and delivery might require some shift in the current paradigm, which is to have the testing and delivery performed by an independent group.

[16] Full automation of the processing would not be without challenges. Cancelled, missing, or delayed raw darks are a significant source of trouble, and an automated pipeline would need to handle these in a carefully planned manner. The /grp/hst disk server caused instability and frequent crashes during processing – better computing hardware might also be needed.

hot pixels that runs to far fainter values. For example, the histogram in Figure 17 shows there are many hot pixels between about 0.005 e-/sec and 0.015 e-/sec that stand out from the noise and background dark current distribution. Also in comparing Figure 15 and Figure 19 we see there are many weak hot pixels which are omitted from the current reference files. Prior to post-flashing the dark frames (e.g. Figure 5), the dark frames contained many artifacts at lower count levels, especially far from the amplifier, but this is no longer the case.

Lowering the threshold for including hot pixels would primarily benefit long exposures in narrow or UV filters where the background counts were low. For example, a 1200 sec post-flashed science exposure might have a background noise level of about 4.6 e- (including read noise and the post-flash), while hot pixels just below the 0.015e-/sec cutoff contribute 18 e- pixels, or 4-sigma events. For dithered images these hot pixels effectively become a noise source, but in this case a significant one. For example, 3.6% of the pixels fall between dark currents of 0.010 and 0.015 e-/sec – this percentage clearly exceeds the 4-sigma noise tail from the combined read noise and post-flash, and would be a potential source of artifacts and noise in the calibrated and stacked image.

However, the benefit for long exposures in broad filters would be more modest. For example, in a 1200 sec exposure with 64 e- of background light, the hot pixels below the threshold contribute 18 e- pixels while the background noise level is about 8 e-. Hence these un-corrected hot pixels represent ~2-sigma events imposed on 3.6% of the pixels, which is similar to the tail of the noise distribution already present in the images.

A middle-ground between the current processing and lowering the threshold would be to have a threshold that ramps down from 0.015 e-/sec to a lower value far from the amplifier. This would at least provide a uniform density of hot pixels in the reference files.

While we have made great improvements by post-flashing the raw dark frames, the effects of CTE losses are still significant. As Figure 10 shows, large numbers of hot pixels are still being lost during read out. And there is still trailing of the brightest hot pixels, as seen in Figure 15. Optimal dark subtraction will occur when the science image and raw dark frames have similar CTE effects, and hence similar background levels. Hopefully most observers are applying adequate post-flash to their images, so there should not be many images with background levels much below the 12 e- post-flash we apply to the raw dark frames. However, long exposures in broad filters can potentially have backgrounds of 60 e- or more, and will have very different CTE losses compared to the dark reference files. One solution would be to have background-dependent dark reference files – i.e. take raw dark frames with several different background levels, but this would require taking more dark frames on-orbit and significant changes to the calibration software. Another approach would be to use a higher post-flash (e.g. 20 e- or more), though this would give poorer calibration for low-background

images, increase the noise, and diverge from the advice we give observers. A better approach might be to apply pixel-based CTE corrections to both the raw dark frames and raw science images, in hopes that this will eliminate CTE effects. Future work is needed to study this possibility and evaluate the degree to which it improves hot pixel subtraction.

Trapping sites in the CCDs create dark pixels in images with significant background levels. We saw these in stacked post-flashed, stacked dark frames (e.g. Figure 14 and Figure 15, and the histogram in Figure 17).These do not have any direct effect on the dark reference files, but it may be useful to consider their calibration and removal from science images.

Summary

We have described the generation and properties of 196 WFC3 dark reference files delivered for Cycles 19 and 20 (approx. from Nov 2011 to Nov. 2013). Dark reference files are produced following each monthly CCD anneal and at 4-day intervals to track the ever-changing hot pixel population. Three different procedures were used during this time: The Type 1 procedure used un-flashed dark frames with files being delivered several months after the observations. Starting at the end of Feb. 2012 the Type 2 procedure emphasized rapid turn-around with reference files being delivered within about 2 weeks of the observations. Type 3 reference files use raw dark frames with a 12 e- post-flash and were delivered for observations in Nov. 2012 and later; these also have continued emphasis on rapid turn-around and delivery of reference files.

The properties of the Type 1 and 2 reference files are very similar, while the Type 3 files have greatly reduced CTE losses. These losses cause hot pixels to be smeared out and lost during readout of the CCDs, and approximately ¾ of the hot pixels are lost in regions far from the CCD amplifier for the Type 1 and 2 files. For Type 3 reference files these losses are reduced to ~43%.

The long-term evolution of the dark current is monitored using plots of the fraction of hot pixels and median (background) dark current, but as we demonstrate, these traditional plots are strongly affected by CTE losses. We suggest some alternate monitoring plots where only the first 100 rows of the CCD are examined, hence reducing the impact of CTE on the statistics. These alternate statistics show the short-term growth of temporary hot pixels (removable by anneal procedures) has remained at about 0.4% per month throughout the WFC3 mission. The long-term growth of permanent hot pixels is constant at about 0.5% per year, and reaches about 2.2% by the end of Cycle 20 (late 2013). The median (background)

dark current increased from ~2 e-/hr/pixel at the start of the WFC3 mission to ~6 e-/hr/pixel by Nov. 2013. Two of the monthly anneals apparently failed and removed few hot pixels, but this had no long-term ill effects – in each case subsequent anneals were successful and returned the hot pixel population to expected levels.

Areas for future improvements are suggested, including further automation of the processing, improved monitoring plots, lowering the 0.015 e-/sec threshold for including hot pixels in the reference files, and further reduction of CTE effects on the dark calibration.

We thank Sylvia Baggett and Jay Anderson for helpful discussions, and Tiffany Borders for assistance in learning the Type 1 procedure. Sylvia Baggett provided detailed comments on this report prior to publication.

References

Anderson, J., Mackenty, J., Baggett, S., and Noeske, K., 2012, "The Efficacy of Post-Flashing for Mitigating CTE-Losses in WFC3/UVIS Images," white paper available at http://www.stsci.edu/hst/wfc3/ins_performance/CTE/ANDERSON_UVIS_POSTFLASH_EFFICACY.pdf

Baggett, S., Bourque, M., Biretta, J., Wheeler, T., Hickey, D., and Swain, S., 2013, "Anomalous Monitor Results After the Aug 2012 Anneal," TIR WFC3 2013-01.

Biretta, J. and Baggett, S., 2013, "WFC3 Post-Flash Calibration," ISR WFC3 2013-12.

Biretta, J., 2014, "WFC3 Cycle 19 & 20 Dark Calibration: Part II," TIR WFC3 2014-01.

Borders, T., Baggett, S., Martel, A. R., and Bushouse, H., 2009, "The WFC3/UVIS Reference Files: 3. Updated Biases and Darks," ISR WFC3 2009-09.

Borders, T. and Baggett, S., 2009, "WFC3 SMOV Proposals 11419, 11426, 11431, and 11446: On-Orbit Darks," ISR WFC3 2009-16.

Bourque, M., et al., 2014, in preparation.

Martel, A. R., Baggett, S., Bushouse, H., and Sabbi, E., 2008, "The WFC3/UVIS Reference Files: 1. The Scripts," TIR WFC3 2008-01.

Martel, A. R., Baggett, S., Bushouse, H., and Sabbi, E., 2009, "The WFC3/UVIS Reference Files: 2. Biases and Darks," ISR WFC3 2008-42.